Widespread male-female expression imbalance of X-linked genes across phrynosomatid lizards

Matthew D. Hale[1,2,*], Pietro L. H. de Mello[1], Daniel T. Nondorf[1], Christopher D. Robinson[1,3], Henry B. John-Alder[4], Christian L. Cox[5], and Robert M. Cox[1,*]

[1] Department of Biology, University of Virginia, Charlottesville, VA 22904

[2] U.S. Military HIV Research Program, Walter Reed Army Institute of Research, Silver Spring, MD 20910; Henry M. Jackson Foundation for the Advancement of Military Medicine, Inc., Bethesda, MD, 20817

[3] School of Life Sciences, Arizona State University, Tempe, AZ 85287

[4] Department of Ecology, Evolution, and Natural Resources, Rutgers University, New Brunswick, NJ 08901

[5] Department of Biological Sciences, Florida International University, Miami, FL 33199

Authors for Correspondence:

*Matthew D. Hale: Washington, DC 20009, USA. Email: matthew.hale.d@gmail.com

*Robert M. Cox: Department of Biology, University of Virginia, Charlottesville, VA, 22904, USA. Phone: 434-982-1987. Email: rmc3u@virginia.edu

Abstract

Classic theory on sex chromosome evolution predicts that selection should restore ancestral diploid expression for hemizygous X-linked genes in males. However, this dosage compensation is often incomplete, leaving X enriched for genes with female-biased expression. In this context, iguanian lizards are noteworthy among vertebrates because several species from separate families appear to exhibit both near-complete dosage compensation and male-female expression balance across their ancient, homologous X chromosomes. We tested for this pattern in a phrynosomatid iguanian, *Sceloporus undulatus* (Eastern Fence Lizard), and instead found that both ancient and more recently sex-linked regions of the X chromosome are enriched for genes with female-biased expression, regardless of age (neonate, maturing, adult) or tissue (brain, liver, muscle). By expanding our analysis across 10 phrynosomatid species spanning 4 genera, we found that male-female expression imbalance on the ancestral region of X is phylogenetically conserved. We also found that an inferred chromosomal rearrangement in the *S. jarrovii* lineage has resulted in the novel acquisition of female-biased expression by a formerly autosomal region. Whereas sex-biased expression of the ancestral region of X is primarily due to females overexpressing X-linked genes relative to autosomal genes, sex-biased expression of these formerly autosomal genes in *S. jarrovii* is primarily due to males underexpressing this putative neo-X region. We conclude that male-female expression imbalance on X is widespread across phrynosomatids, potentially reflecting both overexpression in females for ancestral regions that have evolved dosage compensation and underexpression in males for neo-X regions in which dosage compensation has yet to evolve.

Keywords: autosome, dosage compensation, sex-biased gene expression, sex chromosome, transcriptome

Introduction

The evolution of sex chromosomes poses a recurring challenge because sex-limited Y or W chromosomes typically degenerate due to the suppression of recombination with formerly homologous X or Z chromosomes, resulting in the loss of functional gene content on Y or W (Charlesworth 2021; Graves 2016; Saunders and Muyle 2024). Consequently, genes on X or Z become hemizygous in the heterogametic sex, potentially disrupting protein stoichiometry with autosomal gene products and thus eliciting negative effects on cell function and organismal fitness (Bachtrog et al. 2011; Birchler et al. 2005; Mank 2009; Shaw and White 2022; Veitia and Potier 2015). Classic theory by Ohno (1967) predicts that this deleterious hemizygous state should favor the evolution of compensatory mechanisms that restore ancestral levels of expression for X- or Z-linked genes in the heterogametic sex (Graves 2016; Gu and Walters 2017). Although such dosage compensation has evolved in many taxa, sex chromosomes are nonetheless often enriched for genes with sex-biased expression (Albritton et al. 2014; Chen et al. 2020a; Furman et al. 2020). While this enrichment could indicate that sex chromosomes are hotspots for genes with sexually antagonistic fitness effects (Allen et al. 2013; Dean and Mank 2014), it is primarily thought to occur because dosage compensation is incomplete and evolves on a gene-by-gene basis (Chen et al. 2020a; Darolti et al. 2019; Furman et al. 2020; Gu and Walters 2017; Mank 2013, 2009; Mullon et al. 2015), or because dosage compensation in the heterogametic sex results in the overexpression of X- or Z-linked genes in the homogametic sex (Allen et al. 2013; Bista et al. 2021; Mank et al. 2011; Prince et al. 2010; Wright and Mank 2012). This underscores a key distinction between "sex-chromosome dosage compensation" (*i.e.,* equal expression of X or Z relative to autosomes in the heterogametic sex) and "male-female expression balance" (*i.e.,* equal expression of X or Z in the heterogametic sex relative to X or Z

69 in the homogametic sex) as two separate phenomena (Bista et al. 2021; Disteche 2012; Gu and
70 Walters 2017; Mank 2009).

71 Although some species exhibit both dosage compensation and male-female expression
72 balance (Lucchesi and Kuroda 2015; Metzger et al. 2021; Vicoso and Bachtrog 2015), others
73 appear to lack dosage compensation despite male-female balance (Albritton et al. 2014; Gu et al.
74 2017; Pessia et al. 2014); lack male-female balance despite dosage compensation (Allen et al.
75 2013; Muyle et al. 2018; Prince et al. 2010; Schultheiß et al. 2015); or lack both dosage
76 compensation and male-female balance (Chen et al. 2014; Itoh et al. 2010; Mank 2013).
77 Therefore, many exceptions to Ohno's (1967) pioneering theory of dosage compensation have
78 emerged, and complete dosage compensation across the entire X or Z chromosome is now
79 considered the exception rather than the rule (Chandler 2017; Chen et al. 2020a; Furman et al.
80 2020; Gu and Walters 2017; Mank 2022, 2013, 2009). Overall, dosage compensation appears to
81 be more common in XY than in ZW systems, but the generality of this trend varies across
82 lineages and its potential underlying causes are unclear (Gu and Walters 2017; Mank 2013;
83 Mullon et al. 2015; Vicoso et al. 2013b). One limitation of our current understanding of dosage
84 compensation and male-female expression balance is that it is derived from a relatively limited
85 diversity of taxa (Chen et al. 2020a; Gu and Walters 2017; Kratochvil et al. 2021; Saunders and
86 Muyle 2024). To help address this limitation, we tested for dosage compensation and male-
87 female expression balance across a large reptile lineage with ancestral XY sex-determination.

88 Squamate reptiles (lizards and snakes) are a promising group for studies of dosage
89 compensation because they have repeatedly evolved both XY and ZW sex determination, vary
90 widely in the extent of sex chromosome degeneration and heteromorphism, and exhibit frequent
91 rearrangements between sex chromosomes and autosomes (Alam et al. 2018; Deakin and Ezaz

92 2019; Gamble et al. 2015; Giovannotti et al. 2017; Leaché et al. 2016; Lisachov et al. 2021;
93 Pennell et al. 2015). Yet, dosage compensation and male-female expression balance have only
94 been characterized in a few squamate reptiles, primarily due to the historical lack of high-quality
95 genome assemblies (Pinto et al. 2023). In the viperid rattlesnakes *Crotalus viridis* and *Sistrurus*
96 *miliarius*, dosage compensation is partial and the Z chromosome lacks male-female expression
97 balance (Schield et al. 2019; Vicoso et al. 2013a). Likewise, the varanid lizard *Varanus*
98 *komodoensis* and the related helodermatid lizard *Heloderma suspectum* share a homologous Z
99 chromosome that lacks both dosage compensation and male-female expression balance
100 (Rovatsos et al. 2019; Webster et al. 2024). Similarly, the corytophanid lizard *Basiliscus vittatus*
101 and the pygopodid lizard *Lialis burtonis* each have different X chromosomes that lack male-
102 female expression balance (Acosta et al. 2019; Nielsen et al. 2019; Rovatsos et al. 2021).
103 In contrast to the lack of dosage compensation and expression balance that characterizes
104 many squamates, the anolid lizard *Anolis carolinensis* is one of the few vertebrates to exhibit
105 near-complete dosage compensation and male-female expression balance on its X chromosome
106 (Chen et al. 2020a; Marin et al. 2017; Rovatsos and Kratochvíl 2021; Rupp et al. 2017). Dosage
107 compensation and expression balance in *A. carolinensis* involve an epigenetic mechanism for
108 male-specific upregulation of X that is reminiscent of that found in *Drosophila* (Marin et al.
109 2017). Interestingly, recent data from the phrynosomatid lizard *Urosaurus nigricaudus,* which
110 has an X chromosome homologous to that of *Anolis carolinensis*, suggest the presence of both
111 dosage compensation and male-female expression balance (Davalos-Dehullu et al. 2023). This
112 raises the question of whether the dosage compensation and male-female expression balance
113 observed in *Anolis carolinensis* is conserved across phrynosomatids and other iguanian lineages
114 in the large Pleurodonta clade (>1,250 species). With the exception of corytophanids, all families

115 in Pleurodonta (including the anolids and phrynosomatids mentioned above) share an ancestral
116 XY system that arose over 100 Mya and is thus comparable in age to the ancient eutherian and
117 monotreme XY systems and the avian and ophidian ZW systems (Acosta et al. 2019; Altmanova
118 et al. 2018; Davalos-Dehullu et al. 2023; Marin et al. 2017; Nielsen et al. 2019; Rovatsos et al.
119 2014b). Regions of this ancient iguanian X chromosome exhibit broad synteny across several
120 anolid and phrynosomatid genomes (Davalos-Dehullu et al. 2023; Geneva et al. 2022; Westfall
121 et al. 2021) and hemizygosity in males of several anolid and phrynosomatid species (Geneva et
122 al. 2022; Rovatsos et al. 2014a), as well as both dosage compensation and male-female
123 expression balance in *A. carolinensis* (Chen et al. 2020a; Marin et al. 2017) and potentially also
124 in phrynosomatids such as *Urosaurus nigricaudus* (Davalos-Dehullu et al. 2023).
125 In this study, we first assessed synteny of the X chromosome between the phrynosomatid
126 lizard *Sceloporus undulatus* and other iguanian genomes, then quantified sex-specific DNA
127 dosage along the *S. undulatus* X chromosome to identify regions of male hemizygosity. Using
128 transcriptomic data from multiple ages and tissues, we identified genes that are consistently sex-
129 biased in their expression in *S. undulatus*, determined their chromosomal locations, and tested for
130 both sex-chromosome dosage compensation and male-female expression balance. We conducted
131 these tests separately for the ancestral region of X that is hemizygous in males and for a small,
132 more recently X-linked region in *S. undulatus* that maps to autosomes in several other
133 phrynosomatids and in *A. carolinensis*. While replicating these tests in a congener, we uncovered
134 the transcriptomic signature of another recently X-linked region in *S. jarrovii*, which we also
135 tested for dosage compensation and male-female expression balance. Using liver transcriptomes
136 from seven *Sceloporus* species and three representatives of other phrynosomatid genera, we
137 characterized broad evolutionary trends in sex-biased gene expression across the putatively

138 homologous region of their ancient iguanian X chromosome, as well as the two more recently X-
139 linked regions identified within *S. undulatus* and *S. jarrovii*. Collectively, these analyses extend
140 our understanding of dosage compensation in squamate reptiles, reveal that male-female
141 expression imbalance is widespread across phrynosomatid lizards, and suggest that male-female
142 expression imbalance can occur in the presence of dosage compensation for ancient X-linked
143 genes, or in the absence of dosage compensation for more recently X-linked genes.
144

145 **Results**

146 The X Chromosome of *S. undulatus* has an Ancient Hemizygous Region and a Neo-X Region

147 Westfall et al. (2021) identified the tenth largest scaffold in the *S. undulatus* assembly
148 (NC_056531.1, 16.86 Mbp, hereafter chromosome 10) as the predicted X chromosome. Our
149 analyses confirm that the majority (15.10 Mbp) of *S. undulatus* chromosome 10 is syntenic with
150 the ancient X chromosome in other iguanian genomes, including the more distantly related
151 anolids *Anolis carolinensis* and *A. sagrei* and the more closely related phrynosomatids
152 *Phrynosoma platyrhinos* and *Urosaurus nigricaudus* (Fig. 1; also see Davalos-Dehullu et al.
153 (2023)). In addition, we found that a small (1.76 Mbp), distal region of *S. undulatus* chromosome
154 10 is syntenic with a portion of a putatively autosomal microchromosome in *Phrynosoma*
155 *platyrhinos* (Fig. 1A), suggesting that this is a more recently X-linked region in *S. undulatus*
156 (*i.e.*, a neo-X region). Targeted BLAST searches of predicted mRNA sequences from this distal
157 region confirmed that individual genes located before 15.10 Mbp on chromosome 10 in *S.*
158 *undulatus* typically map to X in all other iguanians (Fig. 1B), whereas genes located after 15.10
159 Mbp only map to X in closely related *S. tristichus* (formerly considered a subspecies of *S.*
160 *undulatus*) and distantly related *A. sagrei* (due to an independent X-autosome fusion within

161 *Anolis*, see Geneva et al. (2022)). In other phrynosomatids (*U. nigricaudus, P. platyrhinos*) and
162 other distantly related anolids (*A. carolinensis*), genes located after 15.10 Mbp on the *S.*
163 *undulatus* X chromosome map to putative autosomes or unplaced scaffolds (Fig. 1B).
164 Analysis of published whole-genome sequences from 18 female and 11 male *S. undulatus*
165 specimens (Assis et al. 2025) revealed that, as expected, $\log_2$ (male/female) DNA coverage is
166 centered at 0 (equal dosage) across all chromosomes except chromosome 10 (Table S2; Fig. S1),
167 which exhibits values near -1 along most of its length (Fig. 1C). This two-fold higher DNA
168 coverage in females indicates that males are hemizygous for most of chromosome 10, confirming
169 its identify as the X chromosome. However, chromosome 10 exhibits a distinct shift toward
170 values centered on 0 beginning at approximately 14.85 Mbp, slightly before the start of the
171 putative neo-X region at 15.10 Mbp (Fig. 1C). Whereas most genes between 14.85 and 15.10
172 Mbp have DNA coverage ratios near 0, genes located after 15.10 Mbp exhibit a range of values
173 between 0 and -1, suggesting that the homologous neo-Y region may be in the process of
174 degeneration (Fig. 1C). In our subsequent analyses of dosage compensation (below), we
175 excluded the 15 genes located between 14.85 and 15.10 Mbp of chromosome 10 because these
176 genes are ancestrally X-linked (Fig. 1B) but exhibit no evidence of a sex difference in dosage
177 (Fig. 1C), suggesting that they may reside on a pseudoautosomal region (PAR) that is still
178 recombining with its Y homolog.
179
180 <u>The *S. undulatus* Genome Contains Many Putatively X- and Y-Linked Scaffolds</u>
181 Although the *S. undulatus* genome was sequenced from male tissue, the current assembly
182 does not include a formally characterized Y chromosome (Westfall et al. 2021). However, our
183 analyses of unplaced scaffolds revealed 45 annotated genes with mean $\log_2$ (male/female) DNA

184 coverage values greater than 0.5 (i.e., a male bias in depth of coverage; Table S2). We
185 hypothesize that many of these scaffolds, which each contain a single gene and collectively
186 comprise only 0.2 Mbp, may correspond to Y-linked regions of the S. *undulatus* genome. We
187 also found 116 annotated genes on unplaced scaffolds with mean $\log_2$ (male/female) DNA
188 coverage values less than -0.5, potentially corresponding to unassembled regions of the X
189 chromosome (Table S2). Filtering to exclude genes with low coverage (mean < 10 in both sexes)
190 left 44 of these potentially Y-linked genes and 65 of these potentially X-linked genes on
191 unassembled scaffolds (Fig. S1).
192
193 The *S. undulatus* Transcriptome Contains Many Consistently Sex-Biased Genes
194 To characterize male-female expression imbalance in *S. undulatus* without any *a priori*
195 assumptions about genomic location, we conducted genome-wide differential gene expression
196 analyses to identify genes that are consistently sex-biased in their expression across three ages
197 (neonate, maturing, adult) in three distinct tissues (liver, brain, muscle). We reasoned that such
198 consistency is more likely to reflect sex differences in gene dosage than in gene regulation,
199 which is likely to be both age- and tissue-specific. We detected cohorts of significantly
200 differentially expressed genes (DEGs; $P < 0.05$ after correction for false discovery rate) that are
201 consistently female-biased across all ages in the liver ($n = 32$ genes; Fig. 2A-C), brain ($n = 48$;
202 Fig. S2A-C), and muscle ($n = 11$; Fig. S3A-C). We also detected cohorts of DEGs that are
203 consistently male-biased across all ages in the liver ($n = 27$; Fig. 2A-C), brain ($n = 34$; Fig. S2A-
204 C), and muscle ($n = 19$; Fig. S3A-C). These consistently sex-biased DEGs typically exhibit the
205 same patterns of sex bias across tissues (Fig. S4A-I), and many are identified as consistently sex-
206 biased DEGs in more than one tissue (Fig. S4J-K). Consistently female-biased DEGs fall within

207 a relatively narrow range of $\log_2$ FC values corresponding to approximately 1.5 to 2-fold higher
208 expression in females, while consistently male-biased DEGs exhibit a wider range of more
209 extreme $\log_2$ FC values (Figs. S2-S5). Consistently female-biased DEGs are expressed in both
210 sexes, as expected if they are located on the X chromosome, whereas many consistently male-
211 biased DEGs are expressed at low or undetectable levels in females (Fig. S5), as expected if they
212 are located on the Y chromosome.
213
214 The X Chromosome of *S. undulatus* is a Hotspot for Female-Biased Gene Expression
215 The majority (45 of 60) of the consistently female-biased DEGs we identified are located
216 on the X chromosome (Fig. 2D-F; Figs. S2-S3). The remainder (15 of 60) are located on small,
217 unplaced scaffolds, many (9 of 15) of which have $\log_2$ (male/female) DNA coverage values
218 below -0.5, suggesting that they are regions of X that were orphaned during assembly (Table S2).
219 Genes across the X chromosome collectively exhibit a significant female bias in their median
220 expression at 2 of 3 ages in liver (Fig. 2D-F), 3 of 3 ages in brain (Fig. S2D-F) and 1 of 3 ages in
221 muscle (Fig. S3D-F). We found identical results when restricting this comparison to genes in the
222 proximal 14.85 Mbp, ancestrally X-linked region. Plotting sex-biased expression as a function of
223 chromosomal location across the 11 largest scaffolds in the *S. undulatus* genome reveals a single
224 peak of elevated sex bias on the X chromosome that is evident across all ages and tissues (Fig.
225 2G-I; Figs. S2-S3). Consistently female-biased genes are widely distributed across the entire
226 length of the X chromosome and are interspersed with many unbiased genes and several
227 consistently male-biased genes (Fig. 2J; Fig. S6). Of the 6 consistently female-biased DEGs
228 located in the hypothesized neo-X region, 5 exhibit a negative $\log_2$ (male/female) DNA coverage
229 value below -0.25, suggesting that their gametologs on the neo-Y chromosome have degenerated

230 or diverged. Whereas both the proximal 14.85 Mbp (ancestrally X-linked region) and the distal
231 1.76 Mbp (hypothesized neo-X region) of the X chromosome contain consistently female-biased
232 DEGs and exhibit an overall tendency toward female-biased expression (Fig. S6), the
233 intermediate 0.25 Mbp (hypothesized PAR) exhibits virtually no sex-biased expression at any
234 age or in any tissue (Fig. S6). Enrichment of the X chromosome with female-biased genes was
235 recapitulated when we mapped *S. undulatus* reads to the genome of closely related *S. tristichus*
236 (Bedoya and Leaché 2021), which was sequenced from female tissue and therefore lacks any Y-
237 linked sequence in its assembly (Figs. S7-S8, see Supplementary Results).
238
239 Consistently Male-Biased Genes Map to X and to Putative Y-linked Scaffolds in *S. undulatus*
240 The majority (31 of 45) of the consistently male-biased DEGs that we identified are
241 located on small, unplaced scaffolds in the *S. undulatus* assembly (Fig. 2D-F; Figs. S2-S3), most
242 of which (22 of 31) we hypothesized to be Y-linked based on $\log_2$ (male/female) DNA coverage
243 values that are above 0.5 (Table S2). One of these male-biased DEGs (*LOC121918292*, an
244 *RPL6*-like gene) had no detectable DNA reads from females. *RPL6* is Y-linked in *Anolis*
245 *carolinensis* (Marin et al. 2017) and is the putative sex-determining locus in *A. sagrei* (Motley
246 2025). A subset (10 of 45) of consistently male-biased DEGs are located on the X chromosome.
247 Although this could potentially occur if some Y-linked regions co-assembled with X (Westfall *et*
248 *al.*, 2021), all of these male-biased genes on the X chromosome exhibit $\log_2$ (male/female) DNA
249 coverage values near -1 (Fig. 1C), indicating that they are hemizygous in males. A few (4 of 45)
250 consistently male-biased DEGs are located on putative autosomes (Figs. 2D-F; S3D-F).
251
252 The X Chromosome of *S. undulatus* is Overexpressed Relative to Autosomes in Females

253 To determine whether male-female expression imbalance on the *S. undulatus* X
254 chromosome is driven by the lack of dosage compensation in males versus overcompensation in
255 females, we compared the expression of X-linked genes to the expression of autosomal genes
256 separately within each sex. We did this by randomly sampling 1000 contiguous regions of the
257 autosomal genome with the same number of expressed genes as the corresponding regions of X
258 to generate null distributions of median autosomal expression values for each sex, age, and tissue
259 (Fig. 3). In *S. undulatus* males, the median expression of ancestrally X-linked genes on the
260 proximal 14.85 Mbp region of the X chromosome is statistically indistinguishable from the
261 sampled autosomal distributions for liver and trends toward the high ends of the sampled
262 autosomal distributions for brain and muscle (Fig. 3A). In females, the median expression of
263 these same ancestrally X-linked genes trends toward the high ends of the simulated autosomal
264 distributions for liver and muscle and significantly exceeds the simulated autosomal distributions
265 for brain (Fig. 3A). We observed similar patterns for more recently X-linked genes on the distal,
266 1.76-Mbp region of the X chromosome (Fig. 3B). Collectively, these results indicate that female-
267 biased expression across the X chromosome is associated with elevated expression of X-linked
268 genes in females, rather than reduced expression of X-linked genes in males.
269
270 Consistently Sex-Biased Genes Identify a Putative Neo-X Region in *S. jarrovii*
271 To explore the phylogenetic conservation of patterns identified in *S. undulatus,* we also
272 tested for consistently sex-biased genes using liver transcriptomes from *S. jarrovii* that were
273 sampled at three ages (neonate, maturing, adult). We detected 63 DEGs in *S. jarrovii* liver that
274 are consistently female-biased across all ages (Fig. 4A-C), as well as 12 DEGs that are
275 consistently male-biased across all ages (Fig. 4A-C). These consistently female-biased DEGs fall

276 within a relatively narrow range of $\log_2$ FC values that corresponds to approximately 2-fold
277 higher expression in females than in males, consistent with X-linkage, whereas most of the
278 consistently male-biased DEGs are expressed at low or undetectable levels in females, consistent
279 with Y-linkage (Fig. S10). Many (20 of 63) of the consistently female-biased DEGs in *S. jarrovii*
280 map to the X chromosome in *S. undulatus* (Fig. 4D-F), and the median expression of all genes
281 that map to the *S. undulatus* X chromosome is significantly female-biased at all ages in *S.*
282 *jarrovii* (Fig. 4D-F). None of the consistently sex-biased genes in *S. jarrovii* map to the distal
283 1.76-Mbp region of the *S. undulatus* X chromosome (Fig. 4J), and this region exhibits no overall
284 female bias in its expression in *S. jarrovii* (Fig. S11), as expected given that genes in this region
285 map to autosomes in all phrynosomatids other than *S. undulatus* and *S. tristichus* (Fig. 1).
286 Unlike in *S. undulatus*, most of the consistently female-biased DEGs (41 of 63) and half
287 of the consistently male-biased DEGs (6 of 12) that we detected in *S. jarrovii* transcriptomes
288 map to the sixth largest scaffold in the *S. undulatus* assembly (NC_056527.1, hereafter
289 chromosome 6), which is an autosome in *S. undulatus* (Fig. 4D-F). Moreover, nearly all (46 of
290 47) of these consistently sex-biased DEGs fall within a relatively small, 11-Mbp distal region of
291 chromosome 6 (hereafter DR6; Fig. 4J) that exhibits a sharp peak of sex-biased expression
292 similar to that observed on the X chromosome (Fig. 4G-I). Genes on chromosome 6 that fall
293 outside of DR6 exhibit no overall tendency toward sex-biased expression in either *S. jarrovii* or
294 *S. undulatus* (Fig. 5). However, the 156 genes located within DR6 are significantly female-
295 biased in *S. jarrovii*, even when excluding the subset of 46 consistently sex-biased DEGs that we
296 first used to identify this region (Fig. 5B). These 156 genes within DR6, including the 46
297 consistently sex-biased DEGs from *S. jarrovii*, do not exhibit any overall sex bias in DNA
298 coverage (Fig. S1) or expression (Fig. 5B) in *S. undulatus*. Collectively, genes within DR6

299 exhibit expression profiles similar to the X chromosome in *S. jarrovii,* but similar to autosomes
300 in *S. undulatus* (Fig. 5). Our expression data therefore suggest that the *S. jarrovii* X chromosome
301 shares an ancestral 14.85-Mbp region with *S. undulatus,* lacks the 1.76-Mbp region that is more
302 recently X-linked in *S. undulatus* (DR10)*,* but includes an 11-Mbp region that is autosomal in *S.*
303 *undulatus* and more recently X-linked in *S. jarrovii* (DR6).
304
305 The Putative Neo-X Region in *S. jarrovii* Lacks Dosage Compensation in Males
306 Similar to our analyses for *S. undulatus*, we compared the median expression of
307 putatively X-linked genes in *S. jarrovii* (*i.e.,* genes on the ancestrally X-linked 14.85-Mbp region
308 of *S. undulatus* chromosome 10 and the recently X-linked 11-Mbp DR6 region of *S. undulatus*
309 chromosome 6) to simulated null distributions of median autosomal expression in males and
310 females by randomly sampling 1000 contiguous regions of the autosomal genome with the same
311 number of expressed genes as the corresponding X-linked regions. In *S. jarrovii* males, median
312 levels of expression for genes mapping to the ancestrally X-linked region of *S. undulatus*
313 chromosome 10 fall within the simulated distributions for autosomal genes, but lower than the
314 median (Fig. S12A). In *S. jarrovii* females, median levels of expression for these same genes are
315 toward the high end of sampled distributions for autosomal genes (Fig. S12A). Therefore, the
316 overall pattern of female-biased expression for ancestrally X-linked genes in *S. jarrovii* reflects a
317 combination moderate underexpression in males and moderate overexpression in females (Fig.
318 S12A). In both sexes of *S. jarrovii*, the median expression of genes that map to DR10 in *S.*
319 *undulatus* is near the center of the simulated autosomal distribution (Fig. S12B), consistent with
320 the interpretation that this neo-X region in *S. undulatus* is not X-linked in *S. jarrovii.*

321 By contrast, the median expression of genes within DR6 is significantly reduced in *S.*
322 *jarrovii* males when compared to sampled null distributions for autosomal genes for maturing
323 and adult ages and nearly so for neonates (Fig. 6A). In *S. jarrovii* females, the median expression
324 of genes within DR6 is similar to the simulated distributions for autosomal genes at all ages (Fig.
325 6A). In *S. undulatus*, the median expression of genes within DR6 is similar to the simulated
326 distribtions for autosomal genes in both sexes (Fig. 6A). Therefore, DR6 in *S. jarrovii* exhibits
327 the predicted transcriptomic profile for X-linked genes that lack dosage compensation in males,
328 whereas DR6 in *S. undulatus* is expressed at levels comparable to other autosomal genes in both
329 sexes. Paired, inter-species comparisons of *S. jarrovii* and *S. undulatus* homologs on DR6
330 corroborate this interpretation. Homologous genes on DR6 are expressed at comparable levels in
331 females of each species (paired *t*-tests within each age, all $P > 0.16$; Fig. 6B), but at significantly
332 lower levels in *S. jarrovii* males than in *S. undulatus* males (all $P < 0.001$; Fig. 6B).
333
334 Male-Female Expression Imbalance of the Ancestral X is Conserved Across Phrynosomatids
335 To characterize broad evolutionary trends in the expression of sex-linked genes, we
336 combined our expression data from adult livers in *S. undulatus* and *S. jarrovii* with similar RNA-
337 seq data (mapped to the *S. undulatus* genome) from adult livers in 5 other *Sceloporus* species,
338 plus representatives of 3 other phrynosomatid genera (Table S1). Across Phrynosomatidae, we
339 observed female-biased expression of genes mapping to the ancestrally X-linked 14.85-Mbp
340 region of *S. undulatus* chromosome 10, suggesting that this signature of male-female expression
341 imbalance is the ancestral state for this family (Fig. 7A). Median $\log_2$ (male/female) expression
342 ratios across this putatively homologous region of the X chromosome are significantly female-
343 biased in adult liver from 6 of 7 *Sceloporus* species, as well as from all 3 phrynosomatid species

344 representing other genera (Fig. 7A). Moreover, each of the DEGs from this ancestral region of
345 chromosome 10 that are consistently female-biased across ages in *S. undulatus* are nearly always
346 also female-biased in other phrynosomatid species (Fig. 7A). Likewise, the few DEGs from this
347 ancestral region of chromosome 10 that are consistently male-biased across ages in *S. undulatus*
348 also tend to exhibit male-biased expression in other species, although this conservation is
349 somewhat weaker (Fig. 7A).
350
351 Male-Female Expression Imbalance of Neo-X Regions is Restricted to Individual Lineages
352 In contrast to the phylogenetically conserved patterns of sex-biased expression for genes
353 on the ancestrally X-linked region of *S. undulatus* chromosome 10 (Fig. 7A), only *S. undulatus*
354 exhibits female-biased expression of genes on its putative neo-X region comprising the distal
355 1.76 Mbp of chromosome 10 (DR10, Fig. 7B). Moreover, the few genes from DR10 that are
356 consistently female-biased DEGs across ages in *S. undulatus* exhibit no overall tendency for
357 female-biased expression in other species (Fig. 7B). Similarly, only *S. jarrovii* exhibits female-
358 biased expression for genes on its putative neo-X region comprising the 11-Mbp distal portion of
359 chromosome 6 in *S. undulatus* (DR6, Fig. 7C). Likewise, genes from DR6 that are consistently
360 either female- or male-biased DEGs across ages in *S. jarrovii* exhibit no clear conservation of
361 these sex-biased expression patterns across other phrynosomatid species (Fig. 7C). Overall, these
362 evolutionary patterns of sex-biased gene expression indicate that the 1.76-Mbp distal region of
363 chromosome 10 is a recently X-linked region in *S. undulatus* (and closely related species such as
364 *S. tristichus*, Fig. 1B), and that the 11-Mbp distal region of chromosome 6 in *S. undulatus* has
365 also recently become sex-linked in the lineage represented here by *S. jarrovii* (Fig. 7C).
366

Discussion

Recent research on sex chromosomes has emphasized the distinction between dosage compensation (of X or Z with autosomes in the heterogametic sex) and expression balance (of X or Z between the sexes) while noting that associations between the two can differ across lineages (Bista et al. 2021; Gu and Walters 2017; Saunders and Muyle 2024). In *Sceloporus undulatus,* male-female expression imbalance across the ancestral, male-hemizygous region of X appears to be associated with the overexpression of this region (relative to autosomes) in females, rather than its underexpression in males. Although this "Type IV" profile (*i.e.,* dosage compensation without male-female expression balance, following Gu & Walters 2017) has been observed in a variety of taxa (Allen et al. 2013; Muyle et al. 2018; Prince et al. 2010; Schultheiß et al. 2015), several subsequent studies have attributed it to artifacts from microarray data, the inclusion of gonadal tissue, or the lack of appropriate tests for dosage compensation (Gu and Walters 2017; Saunders and Muyle 2024). These first two concerns are not relevant to our study, but it has been proposed that tests for dosage compensation should ideally compare expression between sex-linked genes and their orthologs still in the ancestral autosomal state (Bista et al. 2021; Gu and Walters 2017). Due to the considerable age (>100 Mya) of the iguanian X chromosome that is ancestral to Pleurodonta (Acosta et al. 2019; Davalos-Dehullu et al. 2023; Marin et al. 2017), this would require comparisons across distantly related lineages in which transcriptomic profiles may have diverged considerably over millenia. Instead, by comparing X to null distributions sampled from contiguous autosomal blocks within the same genome (and the same biological replicates), we provide an alternative approach that suggests an overall Type IV expression profile for the ancestral region of the X chromosome in *S. undulatus*. We emphasize that this is a summary categorization across hundreds of X-linked genes that vary considerably in their degrees of male-

390 female expression balance, and potentially also in their corresponding degrees of dosage
391 compensation in males. Individual sex-linked genes can vary in whether they exhibit Type I-IV
392 expression profiles (Saunders and Muyle 2024; Webster et al. 2024), even in squamate reptiles
393 with mechanisms for near-complete dosage compensation, such as *Anolis carolinensis* (Marin et
394 al. 2017; Rupp et al. 2017). Interestingly, the same Type IV pattern of male-female expression
395 imbalance appears to characterize the more recently X-linked distal region of the *S. undulatus* X
396 chromosome (DR10). However, it is unclear whether Y degeneration has proceeded to the extent
397 that males actually require dosage compensation for most of this neo-X region, given that $\log_2$
398 male/female DNA coverage ranges from 0 to -1 for individual genes in DR10 and that not at all
399 genes may actually require compensation given their biological function.

400 In contrast to the ancestral region of the X chromosome, the distal region of *S. undulatus*
401 chromosome 6 (DR6) that we identify as a putative neo-X region in *S. jarrovii* appears to exhibit
402 an overall "Type III" expression profile, corresponding to the lack of dosage compensation in
403 males and the lack of expression balance between sexes. This pattern is common in ZW systems,
404 including other squamate reptiles (Rovatsos et al. 2019; Webster et al. 2024), but rare in XY
405 systems (Gu and Walters 2017; Saunders and Muyle 2024). Nonetheless, our comparisons of
406 DR6 expression against randomly sampled autosomal blocks from *S. jarrovii* and also against
407 orthologs in the ancestral autosomal state in *S. undulatus* both indicate that DR6 in *S. jarrovii* is
408 expressed at typical autosomal levels in females and at substantially lower levels in males. Such
409 Type III expression profiles may correspond to early evolutionary stages in which degeneration
410 of Y has created dosage effects in males, but mechanisms for compensatory upregulation of X
411 have yet to evolve. Likewise, Type IV expression profiles may correspond to later evolutionary
412 stages in which dosage compensation has been achieved via the upregulation of X in males, but

413 male-female expression imbalance persists due to the concomitant upregulation of X in females.
414 Ohno (1967) hypothesized that this state may precede the evolution of mechanisms such as X-
415 inactivation in females, which then restore male-female expression balance (Grant et al. 2012;
416 Marin et al. 2017). However, it is unclear whether "Type I" patterns characterized by dosage
417 compensation and male-female expression balance actually evolve via this proposed sequence,
418 particularly in vertebrates (Gu and Walters 2017; Saunders and Muyle 2024). While many
419 ancestrally X-linked genes do exhibit both dosage compensation and male-female expression
420 balance in *S. undulatus*, it is clear that many others still lack male-female expression balance
421 despite sufficient time for its evolution in this ancient (>100 Mya) XY system.

422 The anolid lizard *Anolis carolinensis* has a *Drosophila*-like epigenetic mechanism for the
423 male-specific upregulation of hemizygous X-linked genes (Marin et al. 2017), producing a Type
424 I pattern of both dosage compensation and male-female expression balance across the majority
425 of the X chromosome (Chen et al. 2020a; Rovatsos and Kratochvíl 2021; Rupp et al. 2017). This
426 is noteworthy as one of the few examples of near-complete dosage compensation accompanied
427 by near-complete male-female expression balance in any vertebrate (Chen et al. 2020a; Metzger
428 et al. 2021; Saunders and Muyle 2024). Intriguingly, recent analyses of the phrynosomatid
429 lizards *Urosaurus nigricaudus* and *U. bicarinatus* suggested both dosage compensation and
430 male-female expression balance across X, raising the possibility that the epigenetic mechanism
431 for male-specifc upregulation of X that was first discovered in *A. carolinensis* may be broadly
432 conserved across these distantly related families in Pleurodonta that share a homologous X
433 chromosome (Davalos-Dehullu et al. 2023). Our results are only partly consistent with this
434 interpretation. Although we find that the ancestral region of X does exhibit complete (brain,
435 muscle) to partial (liver) dosage compensation relative to autosomes in *S. undulatus* males, we

436 also find clear evidence of widespread male-female expression imbalance for this same ancestral
437 region of X across phrynosomatids, including another *Urosaurus* species, *U. ornatus.*
438 This discrepancy between studies is unlikely to reflect differences in the genomes used
439 for read mapping (*U. nigricaudus* versus *S. undulatus*), as both produce clear signatures of male
440 hemizygosity for the ancestral region of X when mapping genomic DNA. However, whereas we
441 set out to explicitly test for differential expression on a gene-by-gene basis by calculating mean
442 male and female expression levels from multiple replicate libraries (n = 5-7 per sex) across
443 multiple ages and tissues, Davalos-Dehullu et al. (2023) derived male-female expression ratios
444 from pairwise combinations of one individual male library against one individual female library
445 (n = 2 libraries total per sex). This difference in methodology and sample size, potentially in
446 combination with our use of isolated tissues (brain, liver, and muscle) rather than tail samples
447 comprised of multiple tissue types (*e.g.,* bone, muscle, skin), may have afforded us greater power
448 and precision for identifying sex-biased expression. Importantly, we note that the majority of
449 genes on X lack sex-biased expression for most ages and most tissues, and several even exhibit
450 consistently male-biased expression despite their hemizygosity in males. Therefore, much of the
451 X chromosome does appear to exhibit both dosage compensation and at least partial male-female
452 expression balance in phrynosomatids, despite the clear lack of male-female expression balance
453 for dozens of individual genes. Even those genes that are consistently female-biased across ages
454 and tissues have mean expression ratios of 1.7 rather than 2-fold, indicating partial expression
455 balance. In this sense, *S. undulatus* and other phrynosomatids appear similar to many other
456 species in which dosage compensation is partial and occurs on a gene-by-gene basis (Furman et
457 al. 2020; Gu and Walters 2017; Mank 2013, 2009; Mank and Ellegren 2009; Mullon et al. 2015).

458 This is true even for the near-complete dosage compensation and male-female expression
459 balance seen in *A. carolinensis* (Marin et al. 2017; Rupp et al. 2017; Saunders and Muyle 2024).
460 Chromosomal fusions are common in *Sceloporus* (Leaché et al. 2016), particularly for
461 sex chromosomes (Lisachov et al. 2021). It has been proposed that pseudoautosomal regions
462 (PARs) on the tips of sex chromosomes may facilitate such fusions by avoiding the creation of
463 multiple sex chromosome systems, since the newly fused, formerly autosomal segment can be
464 transferred to the other sex chromosome (*e.g.*, from X to Y) by recombination (Lisachov et al.
465 2021). Although we cannot assess the structure of the putative X-autosome translocation from
466 chromosome 6 to 10 in *S. jarrovii*, the fusion that formed DR10 in the *S. undulatus* lineage is
467 located adjacent to a small region of ancestrally X-linked genes with balanced DNA coverage
468 and expression between the sexes, suggesting that the fusion occurred at a terminal PAR.
469 Interestingly, many of the same syntenic blocks of genes have been repeatedly involved in
470 fusions with sex chromosomes across squamate reptiles (Lisachov et al. 2021), and the DR10
471 region in *S. undulatus* provides another example of this phenomenon. DR10 maps to a portion of
472 a putatively autosomal michrochromosome in other phrynosomatid genomes, but the entire
473 microchromosome has undergone an independent fusion with X in the anolid *A. sagrei* (Geneva
474 et al. 2022; Giovannotti et al. 2017; Kichigin et al. 2016).
475 Finally, our study illustrates how the transcriptomic signatures of male-female expression
476 imbalance can both generate and test hypotheses about the evolution of sex chromosomes, even
477 in the absence of genomic or karyotypic data. For example, the phylogenetically conserved
478 pattern of male-female expression imbalance for genes that map to the ancestrally X-linked
479 region of *S. undulatus* chromosome 10 supports the hypothesis that this region has remained
480 largely X-linked throughout phrynosomatid evolution, with the possible exception of *S. sleveni*.

481 By contrast, the distal region of chromosome 10 (DR10) only exhibits this signature of male-
482 female expression imbalance in *S. undulatus,* consistent with the hypothesis that this region
483 became X-linked more recently, after the split between lineages that gave rise to *S. undulatus*
484 and *S. virgatus*. Syntenty analyses indicate that this region is also X-linked in *S. tristichus*,
485 suggesting that it fused with the ancestral X chromosome approximately 6-10 Mya based on
486 divergence estimates for these three species (Leaché et al. 2016; Westfall et al. 2021). We also
487 found a strong signature of male-female expression imbalance in *S. jarrovii* for genes that map to
488 a small region of *S. undulatus* chromosome 6 (DR6), and the absence of this signature from all
489 other species in our analysis supports the hypothesis that DR6 is also a recently X-linked region.
490 Given that male-female expression imbalance is pronounced and male expression appears to lack
491 dosage compensation for DR6 in *S. jarrovii*, this may represent a younger neo-X region than
492 DR10. However, our current transcriptome sampling across *Sceloporus* lacks the phylogenetic
493 resolution to estimate its age more precisely. In future comparative work, tests for transcriptomic
494 signatures of male-female expression imbalance could provide an efficient way to identify and
495 date similar X-autosome fusions in this and other lineages, particularly when sequencing tissues
496 or ages that exhibit relatively little sex-biased expression from other regulatory mechanisms.
497

498 **Materials and Methods**

499 Synteny and Dosage of the *S. undulatus* X Chromosome

500 To confirm inferences from several previous studies (Davalos-Dehullu et al. 2023;
501 Westfall et al. 2021), we assessed the synteny of *S. undulatus* chromosome 10 (NC_056531.1)
502 with the genomes of three other iguanian lizards in the Pleurodonta clade that share an ancient
503 (>100 Mya) X chromosome: *Phrynosoma platyrhinos* (GCA_020142125.1, MUOH_PhPlat_1.1,

504 (Koochekian et al. 2022)), *Anolis carolinensis* (GCF_000090745.2, AnoCar2.0, (Alföldi et al.
505 2011)), and *Anolis sagrei* (GCA_025583915.1, AnoSag2.1, (Geneva et al. 2022)). Each of these
506 other three genomes was sequenced and assembled from a female specimen. The ancestral X
507 chromosome for this lineage has undergone multiple fusions with autosomes to form several
508 more recently X-linked strata in *A. sagrei* (Geneva et al. 2022). Given the phylogenetic distance
509 separating the species in our analyses (common ancestor ca. 83 Mya), we determined orthology-
510 based syntenic relationships using the R package *GENESPACE* (Lovell et al. 2022), which aligns
511 amino acid sequences using *DIAMOND2* (Buchfink et al. 2015), identifies orthogroups with
512 *OrthoFinder* (Emms and Kelly 2019, 2015), and determines syntenic regions for each non-
513 reciprocal pair of genomes by collapsing syntenic orthogroups into a pan-genome annotation.
514 *GENESPACE* identified a minimum of 16,657 genes distributed across 15,662 orthogoups in *P.*
515 *platyrhinos* and a maximum of 28,605 genes distributed across 15,458 orthogroups in *A.*
516 *carolinensis* after filtering for overdispersion. We used the *GENESPACE* function 'plot_riparian'
517 to visualize synteny for the *S. undulatus* genome with specific focus on chromosome 10.
518 To precisely resolve synteny of the X chromosome at the same gene-by-gene resolution
519 as our transcriptomic analyses, we conducted BLASTN (Altschul et al. 1990; Madden 2013)
520 searches using the longest annotated transcript for each gene on *S. undulatus* chromosome 10 (*n*
521 = 330 with XM accessions) as a query against the NCBI reference genomes of five other
522 iguanian lizards in Pleurodonta: closely related *Sceloporus tristichus,* which was formerly
523 considered a subspecies of *S. undulatus* (GCA_016801065.1, ASM1680106v1 (Bedoya and
524 Leaché 2021)), the additional phrynosomatids *Urosaurus nigricaudus* (GCA_034509955.1,
525 ASU_Unig_1 (Davalos-Dehullu et al. 2023)) and *Phrynosoma platyrhinos* (GCA_020142125.1,
526 MUOH_PhPlat_1.1 (Koochekian et al. 2022)), and two more distantly related anolids, *Anolis*

527 *sagrei* (GCA_037176765.1, rAnoSag1) and *A. carolinensis* (GCA_035594765.1, rAnoCar3.1).
528 We used default BLASTN parameters with minor modifications (reward = 1, penalty = 2, and
529 word_size = 28) and sorted results by lowest e-value and highest query coverage. Across every
530 search, the top three hits were always from the same gene, so we used the top BLASTN hit for
531 each transcript to infer the chromosomal location of the homologous gene in each of the other
532 five species.

533 To characterize sex differences in dosage, we used NCBI *sratoolkit* v.3.0.5 to download
534 short-read, whole-genome sequences (Illumina paired-end 150 bp reads) from 18 female and 11
535 male *S. undulatus* specimens obtained by Assis et al. (2025) as part of a separate study (NCBI
536 accession numbers SRR12504882 to SRR12504910 within bioproject PRJNA656311). We
537 trimmed adaptors and filtered low-quality reads used *fastp* (Chen et al. 2018) with default
538 settings, then summarized quality control metrics using *multiqc* (Ewels et al. 2016). Samples had
539 a mean duplication rate of 8.8% and we retained a mean of 319 M reads per sample (>95% of
540 input) after filtering. We aligned reads to the *S. undulatus* genome using *bowtie2* (Langmead and
541 Salzberg 2012) with default settings and removed alignments with a mapping quality (MQ) score
542 below 20 using *samtools* (Li et al. 2009). The alignment rate exceeded 95% for all specimens.
543 We estimated per-base pair depth of coverage for each individual with 'genomeCoverageBed'
544 and calculated the mean depth of coverage for each sex over non-overlapping 100-kbp windows
545 across the entire genome using 'map' from *bedtools* (Quinlan and Hall 2010). To correct for
546 differences in sequencing depth across individuals, we weighted each 100-kbp window value by
547 the genome-wide mean depth of coverage for that individual using custom *awk* functions.
548 Individuals were sequenced at 54x coverage on average, with normalized depth of coverage

549 ranging from 0.88 (chromosome 11) to 1.02 (chromosome 8) in females and 0.56 (chromosome
550 10) to 1.03 (chromosome 8) in males.

551 To calculate a per-gene weighted coverage value, we first divided the mean coverage
552 depth across the open reading frame of each gene by the mean depth of coverage of its
553 chromosome or scaffold in each individual. Next, we caculated the mean weighted coverage per
554 gene, per sex. We then calculated $\log_2$ (mean weighted coverage in males + 0.001 / mean
555 weighted coverage in females + 0.001) for each gene, which we refer to as $\log_2$ (male/female)
556 coverage. X-linked genes that are hemizygous in males should have $\log_2$ (male/female) coverage
557 values near -1. Although the *S. undulatus* genome was sequenced from a male specimen, it does
558 not contain an assembled Y chromosome (Westfall et al. 2021). To identify potential Y-liked
559 genes, we searched for any scaffolds containing at least one annotated gene with a mean $\log_2$
560 (male/female) coverage value greater than 0.5. To identify potential X-liked genes that were not
561 assembled with chromosome 10, we searched for any scaffolds containing at least one annotated
562 gene with a mean $\log_2$ (male/female) coverage value less than -0.5.

563

564 Tissue Collection for Gene Expression

565 To describe sex differences in gene expression, we collected tissues immediately upon
566 capture of wild animals in their natural habitats. All procedures were reviewed and approved by
567 the Institutional Animal Care and Use Committees at the University of Virginia (protocol 3896),
568 Florida International University (IACUC-20-012-CR01), and Rutgers University (PROTO
569 201800157). Animals were collected under permits from Arizona Game and Fish (SP658032 and
570 SP407104), Texas Parks and Wildlife (SPR-0719-113), and New Jersey Fish and Wildlife (SC
571 2019007). Additional collecting and land use permissions were obtained from Catalina State

572 Park (AZ), the Coronado National Forest branch of the United States Forest Service (AZ),
573 Tucson Parks and Recreation (AZ), Dalquest Desert Research Station (TX), and Colliers Mills
574 Wildlife Management Area (NJ). Collecting locations are provided in Table S1.

575 We collected *S. undulatus* and *S. jarrovii* at each of three ages: neonate, maturing, and
576 adult (n = 5-7 individuals per age, per sex; Table S1). Neonates were collected within several
577 weeks of hatching in oviparous, spring-breeding *S. undulatus* (early September, age <1 mo) and
578 within several weeks of birth in viviparous, fall-breeding *S. jarrovii* (mid June, age <1 mo).
579 Maturing individuals were sampled when sex differences in growth, coloration, and circulating
580 testosterone first emerge in the summer after hatching in *S. undulatus* (July, age 10-11 mo) and
581 the first fall breeding season after birth in *S. jarrovii* (late September, age 4-5 mo) (Cox and
582 John-Alder 2007, 2005; Cox et al. 2005). Reproductive adults were sampled during the breeding
583 season in both *S. undulatus* (mid May, age >20 mo) and *S. jarrovii* (late September, age >16
584 mo). To assess the evolution of sex-biased gene expression, we also collected reproductive adults
585 of five additional *Sceloporus* species (*S. clarkii, S. magister, S. merriami, S. slevini, S. virgatus*)
586 and three species representing other phrynosomatid genera (*Cophosaurus texanus, Urosaurus*
587 *ornatus*, *Uta stansburiana*; n = 6 per sex, per species). Adults of each species were sampled in
588 late April or early May during their breeding seasons (Table S1).

589 We captured lizards by hand or using a hand-held pole with a loop of braided fishing line,
590 then immediately measured them for mass (nearest 0.1 g) and snout-vent length (nearest 1 mm).
591 Sex was determined according to presence or absence of enlarged post-anal scales (present only
592 in males) and confirmed by inspection of the gonads during tissue collection. Immediately
593 following measurement, we euthanized lizards via decapitation and collected liver, whole brain,

594 and muscle (along the femur) into RNAlater (Qiagen, Valencia, CA, USA) on ice. Tissues were
595 held overnight at 4°C, frozen at -20°C, and then stored at -80°C until RNA extraction.
596
597 RNA Extraction and Sequencing
598 We extracted total RNA from liver for all 10 species (Table S1). For *S. undulatus* and *S.*
599 *jarrovii*, this included three age groups (neonate, maturing, and adult). For *S. undulatus*, we also
600 extracted RNA from brain and muscle from all three age groups. RNA was extracted using the
601 Illustra/Cytiva RNAspin Mini RNA Isolation Kit (Global Life Sciences Solutions USA,
602 Marlborough, MA, USA), following the manufacturer's protocol, with the exception that all
603 tissues were homogenized twice (45 s per round at 30 Hz) in lysis buffer using 5-mm stainless
604 steel beads in a Tissuelyser II bead mill (Qiagen; Germantown, MD, USA). We assessed RNA
605 concentrations for all samples using a Nanodrop spectrophotometer (ThermoFisher Scientific,
606 Waltham MA, USA). We also assessed RNA quality and concentration for most samples on an
607 Agilent Bioanalyzer (RNA 6000 Pico; Agilent Biotechnologies, Santa Clara, CA, USA). All
608 samples exhibited sufficient quality for library preparation and sequencing (mean RIN = 8.1).
609 Preparation of cDNA libraries and RNA sequencing was carried out by the Georgia
610 Genomics and Bioinformatics Core at the University of Georgia (Athens, GA, USA). Libraries
611 were prepared using the KAPA Stranded mRNA-Seq kit for Illumina platforms with poly(A)
612 selection (KAPA Biosystems; Wilmington, MA, USA). Library preparation and sequencing were
613 conducted in three batches with respect to species and tissue (Table S1) to optimize comparisons
614 between sexes and to obtain approximately 20 M reads per sample. In the first batch, libraries for
615 *S. undulatus* and *S. jarrovii* liver from all three ages were prepared together using ~1 μg total
616 RNA per sample. In the second batch, libraries for *S. undulatus* brain and muscle from all three

617 ages were prepared using ~2 μg total RNA (brain) or ~0.5 μg total RNA (muscle), with libraries
618 from each tissue loaded in equimolar ratios for sequencing. In the third batch, libraries for *S.*
619 *virgatus, S. clarkii, S. slevini, S. magister, S. merriami*, *U. ornatus*, *U. stansburiana*, and *C.*
620 *texanus* liver from adults were prepared using ~1 μg total RNA. Each batch was sequenced twice
621 on Illumina P3 flow cells (paired-end, 100-bp reads) using an Illumina NextSeq 2000.
622
623 Read Count Generation and Differential Expression Analysis
624 All RNAseq reads were assessed for quality and trimmed using *fastp* (Chen et al. 2018)
625 with paired-end base correction, low-complexity filtering, and 3' end tail quality trimming
626 (average phred score threshold = 20 and window size = 5). Poly(g) and poly(x) trimming were
627 also enabled to remove low complexity sequences from the 3' end of reads, along with an overall
628 minimum length filter of 36 bp and minimum phred quality threshold of 25. Cleaned read pairs
629 and reads orphaned during trimming (*i.e.*, read partner removed due to length or quality) were
630 aligned to the *S. undulatus* genome (GCA_019175285.1; SceUnd_v1.1) using *subread-align*
631 (Liao et al. 2013b) with *S. undulatus* RefSeq coding sequences (GCF_019175285.1) as a guide
632 during alignment (accessed via NCBI). Although we used the *S. undulatus* genome as a common
633 reference to generate comparable read counts across all 10 species, we note that the genus
634 *Sceloporus* exhibits widespread chromosomal evolution (Leaché et al. 2016), such that gene
635 locations in other species may differ from those in the *S. undulatus* assembly.
636 For all reads from *Sceloporus* species, we used default parameters in *subread-align* to
637 identify valid alignments to coding regions in the *S. undulatus* genome. For *Urosaurus*, *Uta*, and
638 *Cophosaurus*, we relaxed alignment stringencies due to increased phylogenetic distance and
639 reduced alignment rates observed when default parameters were used. This entailed a lower

640 minimum number of subreads necessary to report an alignment (-m 2), an increased number of
641 mismatches allowed (-M 5), a lower minimum fragment size (-d 35), an increased maximum
642 fragment size (-D 750), and an increased maximum number of indels (-I 7). Paired reads and
643 reads orphaned during *fastp* trimming were aligned independently and expression counts for all
644 species were generated from alignments using *featureCounts* (Liao et al. 2013a) with default
645 parameters. We summed expression counts from paired reads and orphaned reads to generate
646 final expression estimates for each sample. Only unique alignments were counted towards the
647 total expression estimate for a gene (*i.e.,* multi-mapping reads were not counted).

648 We conducted differential expression analyses using R (v 4.5.2) (R Core Team, 2019)
649 package *edgeR* (v 4.8.2) (Chen et al. 2016; McCarthy et al. 2012; Robinson et al. 2009;
650 Robinson and Smyth 2007). Prior to analysis, we filtered counts to remove low-expression genes
651 using *edgeR* function 'FiltrByExpr' separately for each tissue within each species (Table S1,
652 "edgeR model"). To identify and remove outlier libraries after low-expression filtering, we
653 applied a TMM (trimmed mean of M-values) normalization to expression counts in *edgeR*, then
654 used a $\log_{10}$ counts-per-million (CPM) transformation to adjust for library size. We used robust
655 PCA on $\log_{10}$ (CPM) values to identify and remove any outlier libraries using R package *rrcov*
656 and function 'PcaGrid' (crit.pca.distance = 0.975) (Chen et al. 2020b). We conducted outlier
657 analyses separately for each tissue within each species. The total numbers of samples passing
658 outlier filtering are reported in Table S1. Following outlier removal, we conducted differential
659 expression analysis using TMM-normalized read counts, which we fit to a negative binomial
660 model (*edgeR* function 'glmQLFit', robust = TRUE) with separate models for each species. We
661 identified sex-biased DEGs (differentially expressed genes) using quasi-likelihood *F*-tests
662 comparing female versus male expression for each species with *edgeR* function 'glmQLFTest'.

663 Within each species, we made pairwise comparisons between sexes for each combination of age
664 and tissue. Genes with a Benjamini-Hochberg *P*-value adjusted for the transcriptome-wide false
665 discovery rate ("FDR") < 0.05 were considered DEGs (Benjamini and Hochberg 1995).
666
667 Testing for Male-Female Expression Imbalance in *S. undulatus*
668 After identifying significantly sex-biased DEGs within each combination of age and tisse,
669 we identified the subsets of genes that are consistently female-biased or consistently male-biased
670 DEGs across all ages within a tissue, then determined the chromosomal locations of these genes
671 in the *S. undulatus* assembly. If consistently female-biased DEGs are the result of male-female
672 dosage imbalance, then these DEGs should map predominantly to chromosome 10, the X
673 chromosome. If consistently male-biased DEGs are the result of Y-linkage, then these DEGs
674 should map predominantly to unplaced scaffolds in the *S. undulatus* assembly, which does not
675 include an assembled Y chromosome but does contain sequence from a male specimen. Mapping
676 of consistently sex-biased DEGs to autosomes (chromosomes 1-9 and 11) would indicate either
677 an error in sex chromosome assembly, or a mechanism for consistently sex-biased expression
678 other than dosage imbalance due to male hemizygosity. As noted above, we assessed $\log_2$
679 male/female DNA coverage for each of these consistently sex-biased DEGs to infer underlying
680 patterns of dosage. We also visually assessed genome-wide patterns of sex-biased expression
681 using Mahattan plots with the $-\log_{10}$ (*P*-value) of differential expression for each gene ordered
682 sequentially by chromosome number and transcriptional start site.
683 As a complementary approach to our DEG analysis, we assessed chromosome-wide
684 patterns of sex-biased expression by using *edgeR* function 'rpkm' to calculate the expression of
685 each gene as FPKM (fragments per kilobase of transcript per million mapped reads) using *S.*

686 *undulatus* gene lengths (GCF_019175285.1). For each tissue, we used Wilcoxon signed-rank
687 tests with a Bonferroni-adjusted alpha (0.05 / 3 = 0.017) to test whether the median sex bias in
688 expression ($\log_2$ male/female FPKM) of genes on chromosome 10 differed significantly from 0.
689 We conducted these analyses both with and without the subsets of consistently sex-biased DEGs
690 previously identified in each tissue (see above). Because the current *S. undulatus* assembly does
691 not include a unique Y scaffold, we could not conduct similar tests for Y-linked expression.
692
693 Reassesssing Male-Female Expression Imbalance in *S. undulatus* Using the *S. tristichus* Genome
694 Because the assembly of the *S. undulatus* X chromosome may have been influenced by
695 homologous reads from Y (Westfall et al. 2021), we repeated our analyses of differential gene
696 expression by aligning RNAseq reads from *S. undulatus* to the genome of a closely related
697 congener (*Sceloporus tristichus,* formerly *S. undulatus tristichus*) that was sequenced exclusively
698 from female tissue (Bedoya and Leaché 2021). Using this assembly should minimize any
699 artifacts potentially introduced by similar X and Y sequences in the *S. undulatus* genome, such
700 as the co-assembly of X and Y gametologs on chromosome 10 or the failure of X gametologs to
701 assemble on chromosome 10. Read alignments and estimates of gene expression were made
702 using subread-align and featureCounts against the *S. tristichus* genome (ASM1680141v1) and
703 gene annotations from Bedoya and Leaché (2021; Sceloporus_tristichus_snow_11.gff3) with the
704 same parameters used during alignment to the *S. undulatus* genome (described above). Results of
705 these analyses are presented in the Supplementary Materials.
706
707 Identification of Potential Gametolog Pairs in *S. undulatus*

708 If males express two formerly allelic copies of the same gene (*i.e.*, X and Y gametologs),
709 then the independent mapping of reads to each gametolog could create the appearance of female-
710 biased expression of the X gametolog for a gene that is otherwise expressed similarly in both
711 sexes. For all genes identified as consistently sex-biased DEGs using the *S. undulatus* genome,
712 we used BLASTN (Madden 2013) to search for similar sequences that could represent potential
713 gametologs. We used the longest annotated transcripts for each consistently female-biased DEG
714 as query sequences and searched them against the *S. undulatus* (taxid:8520) refseq_rna database
715 using default alignment parameters (E-threshold = 0.05; word size = 11; max matches in query =
716 0; match/mismatch scores = 2,-3; gap costs = Existence: 5, Extension: 2) with low-complexity
717 filters enabled. We queried the top 100 hits for each female-biased DEG sequence to identify any
718 located on unassembled scaffolds, then assessed male and female expression levels (FPKM) to
719 identify those with low expression in females, indicating possible Y gametologs. We applied a
720 similar strategy to identify any potential X gametologs for consistently male-biased DEGs,
721 which would be expected to occur on chromosome 10 or unplaced scaffolds. In situations where
722 we identified a potential gametolog pair, we re-assessed patterns of sex bias after pooling reads
723 from each separately assembled region (*i.e.*, summing putative X and Y gametolog reads).
724 Results of these analyses are presented in the Supplementary Materials.
725
726 Comparing X-linked to Autosomal Expression in *S. undulatus*
727 We established null distributions of median autosomal expression by randomly sampling
728 spatially contiguous blocks of the same number of autosomal genes as expressed genes on X. We
729 calculated the median $\log_2$ FPKM expression for each block of genes in each tissue, age, and sex,
730 repeating this random selection process 1000 times throughout the autosomal genome to generate

731 a null distribution of median autosomal expression for each combination of tissue, age, and sex.
732 For each sampling iteration, we selected a contiguous block of genes on the same scaffold
733 (excluding genes on unplaced scaffolds) and arrayed consecutively by start position, similar to
734 the arrangement of genes on X. Each block of autosomal genes was sampled only once to avoid
735 pseudoreplication. We then tested whether the median $\log_2$ FPKM expression of genes on X fell
736 outside the lower 5% or upper 95% quantiles of the corresponding autosomal distribution. If
737 median expression on X falls below the corresponding null distribution of median autosomal
738 expression in males, this would indicate a lack of dosage compensation ("Type III" expression
739 pattern, Gu and Walters 2017). If the median expression of genes on X falls above the
740 corresponding null distribution in females, this could indicate that dosage compensation in males
741 has resulted in overexpression of X in females ("Type IV" expression pattern; Gu and Walters
742 2017). We conducted these tests separately for genes on the ancestrally X-linked, 14.85-Mbp
743 region of chromsosome 10 (n = 231 to 255 expressed genes, depending upon tissue), as well as
744 the more recently X-linked, 1.76-Mbp distal region of chromosome 10 (n = 41 to 46 expressed
745 genes), with null distributions of autosomal expression generated separately for each region
746 based on its number of expressed genes in each tissue.
747
748 Testing for Male-Female Expression Imbalance in *S. jarrovii*
749 For *S. jarrovii*, we used the same methods described above for *S. undulatus* to identify
750 consistently sex-biased genes in the liver (i.e., significant DEGs biased towards the same sex
751 across all three ages), and to test for overall male-female expression imbalance across genes on
752 chromosome 10 in the *S. undulatus* assembly (*i.e.*, significant deviations of median $\log_2$
753 male/female FPKM ratios from 0 using Wilcoxon signed-rank tests with Bonferroni correction

754 for tests across 3 ages). Because the distal 1.76-Mbp portion of *S. undulatus* chromosome 10
755 (DR10) is presumably autosomal in *S. jarrovii*, we tested for male-female expression imbalance
756 separately in DR10 and in the ancestrally X-linked 14.85-Mbp region of chromosome 10, which
757 we expected to be X-linked in both species.

758 Our analyses in *S. jarrovii* unexpectedly uncovered a signal of highly sex-biased
759 expression in genes mapping to a small (~11 Mbp) distal region on chromosome 6 in the *S.*
760 *undulatus* assembly (hereafter "DR6"), so we conducted additional analyses to test whether this
761 region exhibits the transcriptomic signatures of an X chromosome in *S. jarrovii*. We used
762 Wilcoxon signed-rank tests (as described above for chromosome 10) to test whether the median
763 $\log_2$ male/female FPKM expression ratio for genes on DR6 differs from 0, and also to compare
764 (separately within each sex) the median $\log_2$ FPKM expression of genes in DR6 to null
765 distributions of median $\log_2$ FPKM expression for 1000 randomly sampled genes located
766 contiguously in other autosomal regions. For comparison, we conducted similar analyses of DR6
767 in *S. undulatus,* where it is autosomal. To directly test for an evolutionary reduction in
768 expression of DR6 genes in *S. jarrovii* males, as expected if this formerly autosomal region has
769 become X-linked but still lacks complete dosage compensation, we conducted paired (by gene) *t*-
770 tests comparing expression of DR6 homologs between *S. undulatus* and *S. jarrovii*. We predicted
771 that expression of DR6 would be similar in females of each species, but reduced in *S. jarrovii*
772 males relatieve to *S. undulatus* males.

773

774 <u>Characterizing the Evolution of Gene Expression Across Phrynosomatidae</u>

775 We generated liver transcriptomes for adult males and females of 7 *Sceloporus* species,
776 plus representatives of 3 other phrynosomatid genera (n = 5-7 individuals per sex, per species;

Table S1). For species, we tested whether genes that map to the ancestrally X-linked, male-hemizygous, 14.85-Mbp region of chromosome 10 in the *S. undulatus* assembly exhibit female-biased expression. To resolve the evolution of neo-X regions, we also tested whether genes that map to the distal regions of *S. undulatus* chromosome 10 (DR10, putative neo-X region in *S. undulatus*) and chromosome 6 (DR6, putative neo-X region in *S. jarrovii*) exhibit female-biased expression in any other species. For each comparison described above, we used a 1-sample Wilcoxon signed-rank test with Bonferroni correction for the 10 comparisons across species (adjusted alpha = 0.005) to test for male-female dosage imbalance (median $\log_2$ male/female FPKM < 0) of all expressed genes that map to the corresponding regions of the *S. undulatus* assembly. We also conducted similar analyses using only the subsets of consistently female-biased DEGs from chromosome 10 (*i.e.,* DEGs in *S. undulatus* transcriptomes) or DR6 (*i.e.,* DEGs in *S. jarrovii* transcriptomes). We visualized evolutionary patterns in gene expression using a consensus phylogeny based on several sources (Leaché et al. 2016; Pyron et al. 2013).

Acknowledgments

We thank Matt Watson and Tyler Wittman for help with sample collection. We thank the Georgia Genomics and Bioinformatics Core (GGBC) for library preparation and sequencing. The authors acknowledge Research Computing at The University of Virginia (https://rc.virginia.edu) for providing compulational resources and technical support that have contributed to the results reported within this publication. This work was supported by a Collaborative Research award from the U.S. National Science Foundation (IOS 1755134 to CLC, IOS 1754934 to HBJ-A, and IOS 1755026 to RMC). CDR was supported by a Research Traineeship from the U.S. National

Sceince Foundation (NRT-ROL 2021791). PLHM was supported by a Rising Scholars Postdoctoral Fellowship from the University of Virginia.

Data Availability

RNAseq data underlying this article will be made available through the National Center for Biotechnology Information (NCBI) Short Read Archive upon acceptance. Read counts and code, as well as edgeR DEG output and FPKM expression estimates from edgeR, are available via figshare (https://doi.org/10.6084/m9.figshare.30324850).

Literature Cited

Acosta A, et al. 2019. Corytophanids replaced the pleurodont XY system with a new pair of XY chromosomes. Genome Biol Evol. 11(9): 2666-2677. doi: 10.1093/gbe/evz196

Alam SMI, Sarre SD, Gleeson D, Georges A, Ezaz T. 2018. Did lizards follow unique pathways in sex chromosome evolution? Genes. 9(5). doi: 10.3390/genes9050239

Albritton SE, et al. 2014. Sex-biased gene expression and evolution of the X chromosome in nematodes. Genetics. 197(3): 865-883. doi: 10.1534/genetics.114.163311

Alföldi J, et al. 2011. The genome of the green anole lizard and a comparative analysis with birds and mammals. Nature. 477(7366): 587-591. doi: 10.1038/nature10390

Allen SL, Bonduriansky R, Chenoweth SF. 2013. The genomic distribution of sex-biased genes in *Drosophila serrata*: X chromosome demasculinization, feminization, and hyperexpression in both sexes. Genome Biol Evol. 5(10): 1986-1994. doi: 10.1093/gbe/evt145

821 Altmanova M, et al. 2018. All iguana families with the exception of basilisks share sex
822 chromosomes. Zoology. 126(98-102. doi: 10.1016/j.zool.2017.11.007
823 Altschul SF, Gish W, Miller W, Myers EW, Lipman DJ. 1990. Basic local alignment search tool.
824 215(3): 403-410. doi: 10.1016/S0022-2836(05)80360-2
825 Assis BA, et al. 2025. Genomic signatures of adaptation in native lizards exposed to human-
826 introduced fire ants. 16(1): 89. doi: 10.1038/s41467-024-55020-4
827 Bachtrog D, et al. 2011. Are all sex chromosomes created equal? Trends Genet. 27(9): 350-357.
828 doi: 10.1016/j.tig.2011.05.005
829 Bedoya AM, Leaché AD. 2021. Characterization of a pericentric inversion in plateau fence
830 lizards (*Sceloporus tristichus*): evidence from chromosome-scale genomes. G3: Genes,
831 Genomes, Genetics. 11(2). doi: 10.1093/g3journal/jkab036
832 Benjamini Y, Hochberg Y. 1995. Controlling the false discovery rate: A practical and powerful
833 approach to multiple testing. 57(1): 289-300. doi: 10.1111/j.2517-6161.1995.tb02031.x
834 Birchler JA, Riddle NC, Auger DL, Veitia RA. 2005. Dosage balance in gene regulation:
835 Biological implications. Trends Genet. 21(4): 219-226. doi: 10.1016/j.tig.2005.02.010
836 Bista B, Wu Z, Literman R, Valenzuela N. 2021. Thermosensitive sex chromosome dosage
837 compensation in ZZ/ZW softshell turtles, *Apalone spinifera*. Philos Trans R Soc Lond B
838 Biol Sci. 376(1833): 20200101. doi: 10.1098/rstb.2020.0101
839 Buchfink B, Xie C, Huson DH. 2015. Fast and sensitive protein alignment using DIAMOND.
840 Nat Methods. 12(1): 59-60. doi: 10.1038/nmeth.3176
841 Chandler CH. 2017. When and why does sex chromosome dosage compensation evolve? Ann N
842 Y Acad Sci. 1389(1): 37-51. doi: 10.1111/nyas.13307

843 Charlesworth D. 2021. The timing of genetic degeneration of sex chromosomes. Philos Trans R
844 Soc Lond B Biol Sci. 376(1832): 20200093. doi: 10.1098/rstb.2020.0093
845 Chen J, Wang M, He X, Yang JR, Chen X. 2020a. The evolution of sex chromosome dosage
846 compensation in animals. J Genet Genomics. 47(11): 681-693. doi:
847 10.1016/j.jgg.2020.10.005
848 Chen S, et al. 2014. Whole-genome sequence of a flatfish provides insights into ZW sex
849 chromosome evolution and adaptation to a benthic lifestyle. Nat Genet. 46(3): 253-260.
850 doi: 10.1038/ng.2890
851 Chen S, Zhou Y, Chen Y, Gu J. 2018. fastp: an ultra-fast all-in-one FASTQ preprocessor.
852 Bioinformatics. 34(17): i884-i890. doi: 10.1093/bioinformatics/bty560
853 Chen X, Zhang B, Wang T, Bonni A, Zhao G. 2020b. Robust principal component analysis for
854 accurate outlier sample detection in RNA-Seq data. BMC Bioinf. 21(1): 269. doi:
855 10.1186/s12859-020-03608-0
856 Chen Y, Lun AT, Smyth GK. 2016. From reads to genes to pathways: differential expression
857 analysis of RNA-Seq experiments using Rsubread and the edgeR quasi-likelihood
858 pipeline. F1000Res. 5(
859 Cox RM, John-Alder HB. 2007. Growing apart together: The development of contrasting sexual
860 size dimorphisms in sympatric *Sceloporus* lizards. Herpetologica. 63(3): 245-257. doi:
861 10.1655/0018-0831(2007)63[245:Gattdo]2.0.Co;2
862 Cox RM, John-Alder HB. 2005. Testosterone has opposite effects on male growth in lizards
863 (*Sceloporus* spp.) with opposite patterns of sexual size dimorphism. J Exp Biol. 208(24):
864 4679-4687. doi: 10.1242/jeb.01948

865 Cox Robert M, Skelly Stephanie L, John-Alder Henry B. 2005. Testosterone inhibits growth in
866 juvenile male Eastern Fence Lizards (*Sceloporus undulatus*): Implications for energy
867 allocation and sexual size dimorphism. Physiol Biochem Zool. 78(4): 531-545. doi:
868 10.1086/430226
869 Darolti I, et al. 2019. Extreme heterogeneity in sex chromosome differentiation and dosage
870 compensation in livebearers. Proc Natl Acad Sci U S A. 116(38): 19031-19036. doi:
871 10.1073/pnas.1905298116
872 Davalos-Dehullu E, et al. 2023. Chromosome-level genome assembly of the Blacktail Brush
873 Lizard, *Urosaurus nigricaudus*, reveals dosage compensation in an endemic lizard.
874 Genome Biol Evol. 15(12). doi: 10.1093/gbe/evad210
875 Deakin JE, Ezaz T. 2019. Understanding the evolution of reptile chromosomes through
876 applications of combined cytogenetics and genomics approaches. Cytogenet Genome
877 Res. 157(1-2): 7-20. doi: 10.1159/000495974
878 Dean R, Mank JE. 2014. The role of sex chromosomes in sexual dimorphism: Discordance
879 between molecular and phenotypic data. J Evol Biol. 27(7): 1443-1453. doi:
880 10.1111/jeb.12345
881 Disteche CM. 2012. Dosage compensation of the sex chromosomes. Annu Rev Genet. 46(537-
882 560. doi: 10.1146/annurev-genet-110711-155454
883 Emms DM, Kelly S. 2019. OrthoFinder: phylogenetic orthology inference for comparative
884 genomics. Genome Biol. 20(1): 238. doi: 10.1186/s13059-019-1832-y
885 Emms DM, Kelly S. 2015. OrthoFinder: solving fundamental biases in whole genome
886 comparisons dramatically improves orthogroup inference accuracy. Genome Biol. 16(1):
887 157. doi: 10.1186/s13059-015-0721-2

888 Ewels P, Magnusson M, Lundin S, Käller M. 2016. MultiQC: summarize analysis results for
889 multiple tools and samples in a single report. Bioinformatics. 32(19): 3047-3048. doi:
890 10.1093/bioinformatics/btw354
891 Furman BLS, et al. 2020. Sex chromosome evolution: So many exceptions to the rules. Genome
892 Biol Evol. 12(6): 750-763. doi: 10.1093/gbe/evaa081
893 Gamble T, et al. 2015. Restriction site-associated DNA sequencing (RAD-seq) reveals an
894 extraordinary number of transitions among gecko sex-determining systems. Mol Biol
895 Evol. 32(5): 1296-1309. doi: 10.1093/molbev/msv023
896 Geneva AJ, et al. 2022. Chromosome-scale genome assembly of the brown anole (*Anolis sagrei*),
897 an emerging model species. Commun Biol. 5(1): 1126. doi: 10.1038/s42003-022-04074-5
898 Giovannotti M, et al. 2017. New insights into sex chromosome evolution in anole lizards
899 (Reptilia, Dactyloidae). Chromosoma. 126(2): 245-260. doi: 10.1007/s00412-016-0585-6
900 Grant J, et al. 2012. Rsx is a metatherian RNA with Xist-like properties in X-chromosome
901 inactivation. Nature. 487(7406): 254-258. doi: 10.1038/nature11171
902 Graves JA. 2016. Evolution of vertebrate sex chromosomes and dosage compensation. Nat Rev
903 Genet. 17(1): 33-46. doi: 10.1038/nrg.2015.2
904 Gu L, Walters JR. 2017. Evolution of sex chromosome dosage compensation in animals: A
905 beautiful theory, undermined by facts and bedeviled by details. Genome Biol Evol. 9(9):
906 2461-2476. doi: 10.1093/gbe/evx154
907 Gu L, Walters JR, Knipple DC. 2017. Conserved patterns of sex chromosome dosage
908 compensation in the Lepidoptera (WZ/ZZ): Insights from a moth neo-Z chromosome.
909 Genome Biol Evol. 9(3): 802-816. doi: 10.1093/gbe/evx039

910 Itoh Y, et al. 2010. Sex bias and dosage compensation in the zebra finch versus chicken
911 genomes: General and specialized patterns among birds. Genome Res. 20(4): 512-518.
912 doi: 10.1101/gr.102343.109
913 Kichigin IG, et al. 2016. Evolutionary dynamics of *Anolis* sex chromosomes revealed by
914 sequencing of flow sorting-derived microchromosome-specific DNA. Mol Genet
915 Genomics. 291(1955-1966.
916 Koochekian N, et al. 2022. A chromosome-level genome assembly and annotation of the desert
917 horned lizard, *Phrynosoma platyrhinos*, provides insight into chromosomal
918 rearrangements among reptiles. Gigascience. 11(doi: 10.1093/gigascience/giab098
919 Kratochvil L, Gamble T, Rovatsos M. 2021. Sex chromosome evolution among amniotes: Is the
920 origin of sex chromosomes non-random? Philos Trans R Soc Lond B Biol Sci.
921 376(1833): 20200108. doi: 10.1098/rstb.2020.0108
922 Langmead B, Salzberg SL. 2012. Fast gapped-read alignment with Bowtie 2. Nat Methods. 9(4):
923 357-359. doi: 10.1038/nmeth.1923
924 Leaché AD, Banbury BL, Linkem CW, de Oca AN. 2016. Phylogenomics of a rapid radiation: is
925 chromosomal evolution linked to increased diversification in north american spiny lizards
926 (Genus *Sceloporus*)? BMC Evol Biol. 16(63. doi: 10.1186/s12862-016-0628-x
927 Li H, et al. 2009. 1000 genome project data processing subgroup. The sequence alignment/map
928 format and SAMtools. Bioinformatics. 25(16): 2078-2079.
929 Liao Y, Smyth GK, Shi W. 2013a. featureCounts: an efficient general purpose program for
930 assigning sequence reads to genomic features. Bioinformatics. 30(7): 923-930. doi:
931 10.1093/bioinformatics/btt656

932 Liao Y, Smyth GK, Shi W. 2013b. The Subread aligner: fast, accurate and scalable read mapping
933 by seed-and-vote. Nucleic Acids Res. 41(10): e108-e108. doi: 10.1093/nar/gkt214
934 Lisachov AP, et al. 2021. Whole-chromosome fusions in the karyotype evolution of *Sceloporus*
935 (Iguania, Reptilia) are more frequent in sex chromosomes than autosomes. Philos Trans R
936 Soc Lond B Biol Sci. 376(1833): 20200099. doi: 10.1098/rstb.2020.0099
937 Lovell JT, et al. 2022. GENESPACE tracks regions of interest and gene copy number variation
938 across multiple genomes. eLife. 11(e78526. doi: 10.7554/eLife.78526
939 Lucchesi JC, Kuroda MI. 2015. Dosage compensation in *Drosophila*. Cold Spring Harb Perspect
940 Biol. 7(5). doi: 10.1101/cshperspect.a019398
941 Madden T. 2013. The BLAST sequence analysis tool. The NCBI handbook. 2(5): 425-436.
942 Mank JE. 2022. Are plant and animal sex chromosomes really all that different? Philos Trans R
943 Soc Lond B Biol Sci. 377(1850): 20210218. doi: 10.1098/rstb.2021.0218
944 Mank JE. 2013. Sex chromosome dosage compensation: Definitely not for everyone. Trends
945 Genet. 29(12): 677-683. doi: 10.1016/j.tig.2013.07.005
946 Mank JE. 2009. The W, X, Y and Z of sex-chromosome dosage compensation. Trends Genet.
947 25(5): 226-233. doi: 10.1016/j.tig.2009.03.005
948 Mank JE, Ellegren H. 2009. All dosage compensation is local: Gene-by-gene regulation of sex-
949 biased expression on the chicken Z chromosome. Heredity. 102(3): 312-320. doi:
950 10.1038/hdy.2008.116
951 Mank JE, Hosken DJ, Wedell N. 2011. Some inconvenient truths about sex chromosome dosage
952 compensation and the potential role of sexual conflict. Evolution. 65(8): 2133-2144. doi:
953 10.1111/j.1558-5646.2011.01316.x

954 Marin R, et al. 2017. Convergent origination of a *Drosophila*-like dosage compensation
955 mechanism in a reptile lineage. Genome Res. 27(12): 1974-1987. doi:
956 10.1101/gr.223727.117
957 McCarthy DJ, Chen Y, Smyth GK. 2012. Differential expression analysis of multifactor RNA-
958 Seq experiments with respect to biological variation. Nucleic Acids Res. 40(10): 4288-
959 4297. doi: 10.1093/nar/gks042
960 Metzger DCH, Sandkam BA, Darolti I, Mank JE. 2021. Rapid evolution of complete dosage
961 compensation in *Poecilia*. Genome Biol Evol. 13(7). doi: 10.1093/gbe/evab155
962 Motley MK 2025. Uncovering the underlying genetic mechanisms of sex determination, gonad
963 differentiation, and dosage compensation in the brown anole lizard, *Anolis sagrei*.
964 [[Athens, GA]: University of Georgia.
965 Mullon C, Wright AE, Reuter M, Pomiankowski A, Mank JE. 2015. Evolution of dosage
966 compensation under sexual selection differs between X and Z chromosomes. Nat
967 Commun. 6(7720. doi: 10.1038/ncomms8720
968 Muyle A, et al. 2018. Genomic imprinting mediates dosage compensation in a young plant XY
969 system. Nature plants. 4(9): 677-680.
970 Nielsen SV, et al. 2019. Escaping the evolutionary trap? Sex chromosome turnover in basilisks
971 and related lizards (Corytophanidae: Squamata). Biol Lett. 15(10): 20190498. doi:
972 10.1098/rsbl.2019.0498
973 Ohno S. 1967. Sex Chromosomes and Sex-linked Genes. Heidelberg: Springer Berlin.
974 Pennell MW, et al. 2015. Y fuse? Sex chromosome fusions in fishes and reptiles. PLOS Genet.
975 11(5). doi: 10.1371/journal.pgen.1005237

976 Pessia E, Engelstädter J, Marais GAB. 2014. The evolution of X chromosome inactivation in
977 mammals: The demise of Ohno's hypothesis? Cell Molec Life Sci. 71(8): 1383-1394.
978 doi: 10.1007/s00018-013-1499-6
979 Pinto BJ, Gamble T, Smith CH, Wilson MA. 2023. A lizard is never late: Squamate genomics as
980 a recent catalyst for understanding sex chromosome and microchromosome evolution.
981 114(5): 445-458. doi: 10.1093/jhered/esad023
982 Prince EG, Kirkland D, Demuth JP. 2010. Hyperexpression of the X chromosome in both sexes
983 results in extensive female bias of X-linked genes in the flour beetle. Genome Biol Evol.
984 2(336-346. doi: 10.1093/gbe/evq024
985 Pyron RA, Burbrink FT, Wiens JJ. 2013. A phylogeny and revised classification of Squamata,
986 including 4161 species of lizards and snakes. BMC Evol Biol. 13(1): 93. doi:
987 10.1186/1471-2148-13-93
988 Quinlan AR, Hall IM. 2010. BEDTools: A flexible suite of utilities for comparing genomic
989 features. Bioinformatics. 26(6): 841-842. doi: 10.1093/bioinformatics/btq033
990 Robinson MD, McCarthy DJ, Smyth GK. 2009. edgeR: A Bioconductor package for differential
991 expression analysis of digital gene expression data. Bioinformatics. 26(1): 139-140. doi:
992 10.1093/bioinformatics/btp616
993 Robinson MD, Smyth GK. 2007. Moderated statistical tests for assessing differences in tag
994 abundance. Bioinformatics. 23(21): 2881-2887. doi: 10.1093/bioinformatics/btm453
995 Rovatsos M, Altmanova M, Pokorna M, Kratochvil L. 2014a. Conserved sex chromosomes
996 across adaptively radiated *Anolis* lizards. Evolution. 68(7): 2079-2085. doi:
997 10.1111/evo.12357

998 Rovatsos M, et al. 2021. Do male and female heterogamety really differ in expression
999 regulation? Lack of global dosage balance in pygopodid geckos. Philos Trans R Soc
1000 Lond B Biol Sci. 376(1833): 20200102. doi: 10.1098/rstb.2020.0102
1001 Rovatsos M, Kratochvíl L. 2021. Evolution of dosage compensation does not depend on genomic
1002 background. Molec Ecol. 30(8): 1836-1845. doi: 10.1111/mec.15853
1003 Rovatsos M, Pokorna M, Altmanova M, Kratochvil L. 2014b. Cretaceous park of sex
1004 determination: Sex chromosomes are conserved across iguanas. Biol Lett. 10(3):
1005 20131093. doi: 10.1098/rsbl.2013.1093
1006 Rovatsos M, Rehak I, Velensky P, Kratochvil L. 2019. Shared ancient sex chromosomes in
1007 varanids, beaded lizards, and alligator lizards. Mol Biol Evol. 36(6): 1113-1120. doi:
1008 10.1093/molbev/msz024
1009 Rupp SM, et al. 2017. Evolution of dosage compensation in *Anolis carolinensis*, a reptile with
1010 XX/XY chromosomal sex determination. Genome Biol Evol. 9(1): 231-240. doi:
1011 10.1093/gbe/evw263
1012 Saunders PA, Muyle A. 2024. Sex chromosome evolution: Hallmarks and question marks. Mol
1013 Biol Evol. 41(11). doi: 10.1093/molbev/msae218
1014 Schield DR, et al. 2019. The origins and evolution of chromosomes, dosage compensation, and
1015 mechanisms underlying venom regulation in snakes. Genome Res. 29(4): 590-601. doi:
1016 10.1101/gr.240952.118
1017 Schultheiß R, Viitaniemi HM, Leder EH. 2015. Spatial dynamics of evolving dosage
1018 compensation in a young sex chromosome system. Genome Biol Evol. 7(2): 581-590.
1019 doi: 10.1093/gbe/evv013

1020 Shaw DE, White MA. 2022. The evolution of gene regulation on sex chromosomes. Trends
1021 Genet. 38(8): 844-855. doi: 10.1016/j.tig.2022.04.004
1022 Veitia RA, Potier MC. 2015. Gene dosage imbalances: Action, reaction, and models. Trends
1023 Biochem Sci. 40(6): 309-317. doi: 10.1016/j.tibs.2015.03.011
1024 Vicoso B, Bachtrog D. 2015. Numerous transitions of sex chromosomes in Diptera. PLoS Biol.
1025 13(4): e1002078. doi: 10.1371/journal.pbio.1002078
1026 Vicoso B, Emerson JJ, Zektser Y, Mahajan S, Bachtrog D. 2013a. Comparative sex chromosome
1027 genomics in snakes: Differentiation, evolutionary strata, and lack of global dosage
1028 compensation. PLoS Biol. 11(8). doi: 10.1371/journal.pbio.1001643
1029 Vicoso B, Kaiser VB, Bachtrog D. 2013b. Sex-biased gene expression at homomorphic sex
1030 chromosomes in emus and its implication for sex chromosome evolution. Proc Natl Acad
1031 Sci U S A. 110(16): 6453-6458. doi: 10.1073/pnas.1217027110
1032 Webster TH, et al. 2024. Lack of dosage balance and incomplete dosage compensation in the
1033 ZZ/ZW Gila Monster (*Heloderma suspectum*) revealed by de novo genome assembly.
1034 Genome Biol Evol. 16(3). doi: 10.1093/gbe/evae018
1035 Westfall AK, et al. 2021. A chromosome-level genome assembly for the Eastern Fence Lizard
1036 (*Sceloporus undulatus*), a reptile model for physiological and evolutionary ecology.
1037 Gigascience. 10(10). doi: 10.1093/gigascience/giab066
1038 Wright AE, Mank JE. 2012. Battle of the sexes: Conflict over dosage-sensitive genes and the
1039 origin of X chromosome inactivation. Proc Natl Acad Sci U S A. 109(14): 5144-5145.
1040 doi: 10.1073/pnas.1202905109
1041

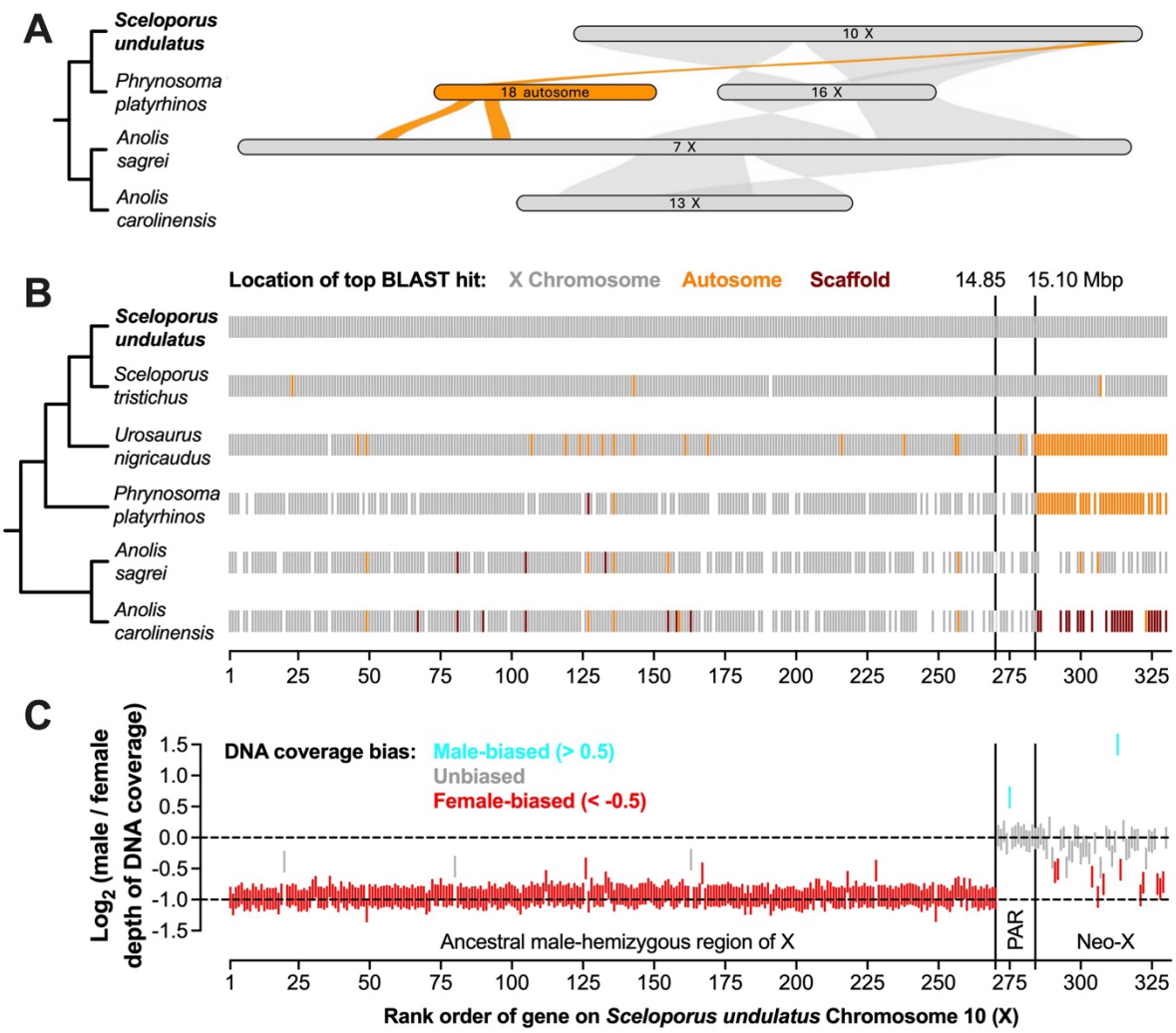

Figure 1. **(A)** Riparian plot illustrating synteny of *S. undulatus* chromosome 10 (X) with three other iguanian genomes. Only chromosome-level scaffolds with syntenic blocks that map to *S. undulatus* chromosome 10 are shown. **(B)** Chromosomal locations of genes on *S. undulatus* chromosome 10 in five other iguanian genomes, based on top BLAST hits using the longest mRNA isoform for each gene as a query. **(C)** Log_2 (male/female) depth of DNA sequencing coverage in *S. undulatus* for each gene on chromosome 10, with the dashed line at -1 signifying expected dosage imbalance due to hemizygosity in males. Vertical lines in **B** and **C** indicate inferred boundaries between the ancestral male-hemizygous region, ancestral psuedoautosomal region (PAR), and neo-X region in *S. undulatus* and *S. tristichus*.

1052 **Figure 2.**

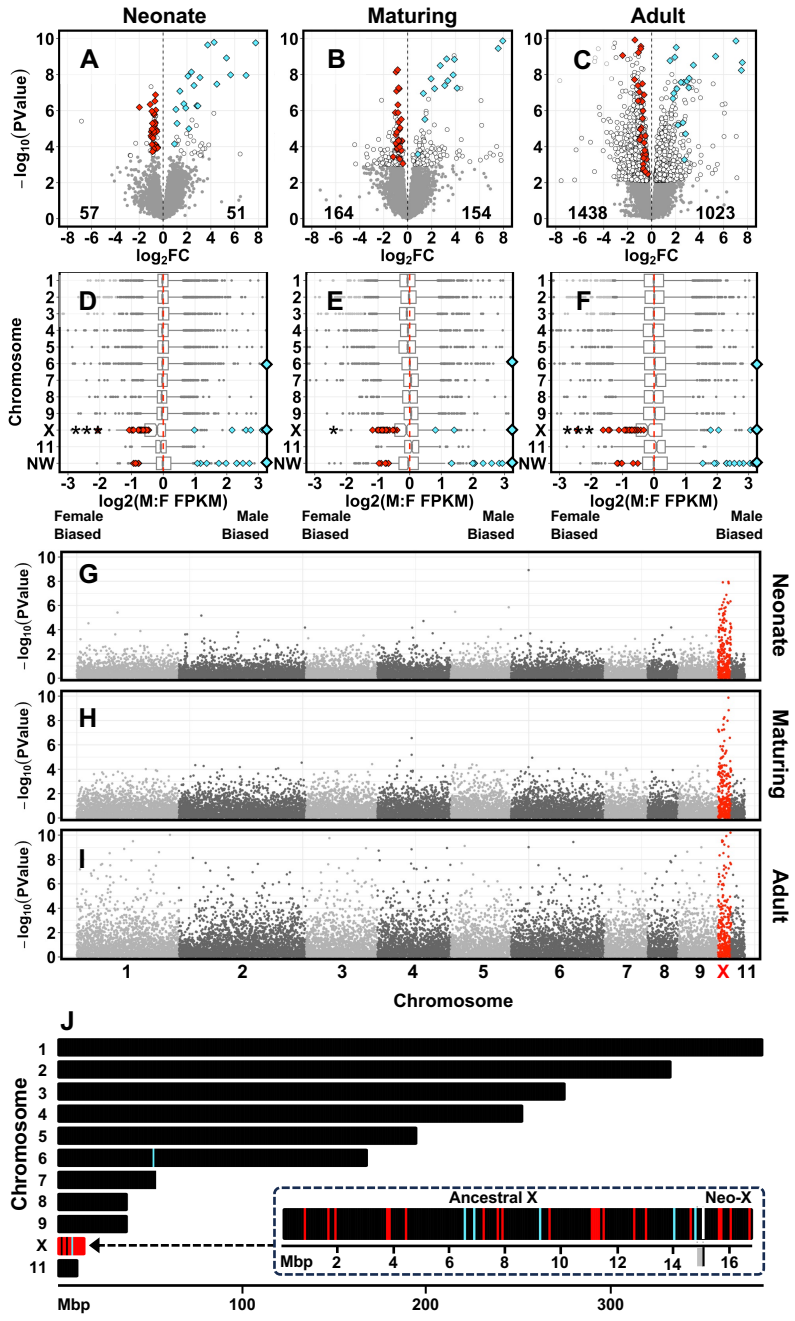

1053

1054 **Figure 2. (A-C)** Volcano plots depicting the magnitude ($\log_2$ fold change) and significance (-
1055 $\log_{10} P$ value) of sex-biased expression across 15,587 genes in liver of *S. undulatus* across three
1056 ages. Genes with significantly (FDR < 0.05) sex-biased expression (DEGs) are indicated in
1057 white, with the number of female-biased and male-biased DEGs indicated in the bottom corners
1058 of each panel. DEGs with consistently sex-biased expression across all ages are shown as red
1059 (female-biased) or blue (male-biased) diamonds. Grey points are genes that are not significantly
1060 sex-biased. **(D-F)** Boxplots depicting the median (line), interquartile range (box) and the smallest
1061 or largest values within 1.5 x IQR (whiskers) for sex-biased expression ($\log_2$ male:female ratio of
1062 fragments per kilobase per million mapped reads, FPKM) from each of the 11 largest scaffolds
1063 and pooled genes from unplaced scaffolds (NW) in the *S. undulatus* assembly. The 10th largest
1064 scaffold is the X chromosome. Notches in the center of each boxplot indicate the 95%
1065 confidence interval of the median. Diamonds indicate consistently female-biased (red) and male-
1066 biased (blue) DEGs in each tissue, which map predominantly to chromosome 10 (X) and
1067 unplaced scaffolds (NW). Diamonds on plot borders indicate DEGs beyond x-axis limits.
1068 Asterisks indicate when median chromosome expression deviates significantly from balanced
1069 male:female expression using Wilcoxon rank sum testing (mu = 0) with correction for multiple
1070 tests (* $P < 0.05$ without correction for multiple tests; ** $P < 0.017$, the critical alpha after
1071 Bonferroni correction; *** $P < 0.001$). **(G-I)** Manhattan plots of $-\log_{10} P$ values for sex-biased
1072 expression after ordering genes by chromosome and start position. All genes on X are shown in
1073 red. **(J)** Genomic locations of consistently sex-biased DEGs (unplaced scaffolds not shown).
1074 Enlarged inset shows that these genes occur on both the ancestral region of X that is hemizygous
1075 in males and on the putative neo-X region beyond the large tick mark at 15.1 Mbp. Gray shading
1076 immediately before this large tick indicates the putative psuedoautosomal region.

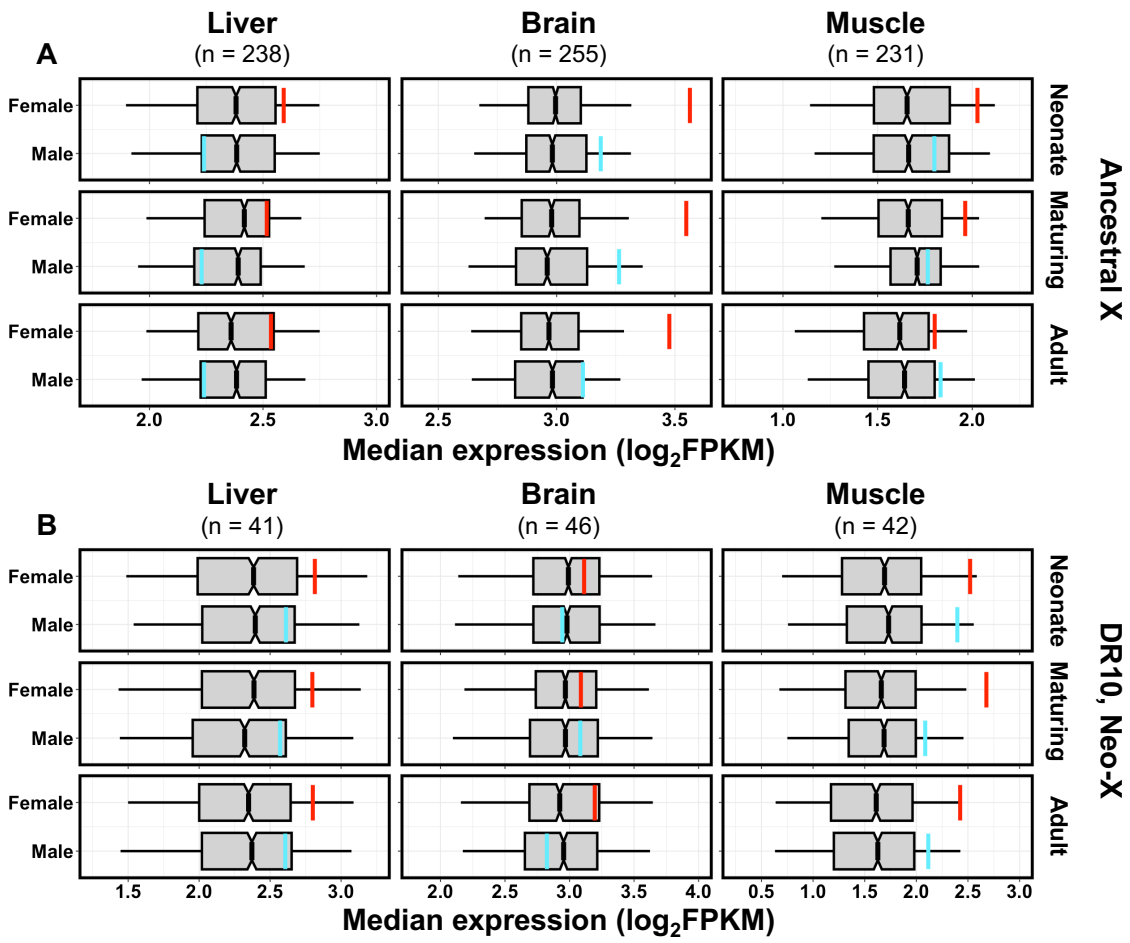

Figure 3. Comparisons of median expression on the X chromosome versus that of autosomes for each sex across three tissues and three ages in *S. undulatus*, shown separately for (**A**) the ancestrally X-linked 14.85-Mbp region of chromosome 10, and (**B**) the distal 1.76 Mbp region (DR10) that is more recently X-linked. Boxplots depict the median (line), IQR (box), and 5th and 95th quantiles (whiskers) for median expression estimates from 1000 randomly-sampled blocks of *n* contiguous autosomal genes (*n* = number of expressed genes in the corresponding region of the X chromosome in that tissue). Colored vertical lines (red = female; blue = male) indicate the median expression of all genes on X for each combination of sex, age, and tissue. Colored lines which fall beyond whiskers indicate that median expression of genes on the X chromosome differs significantly from the sampled distribution for autosomal genes.

1088 **Figure 4.**

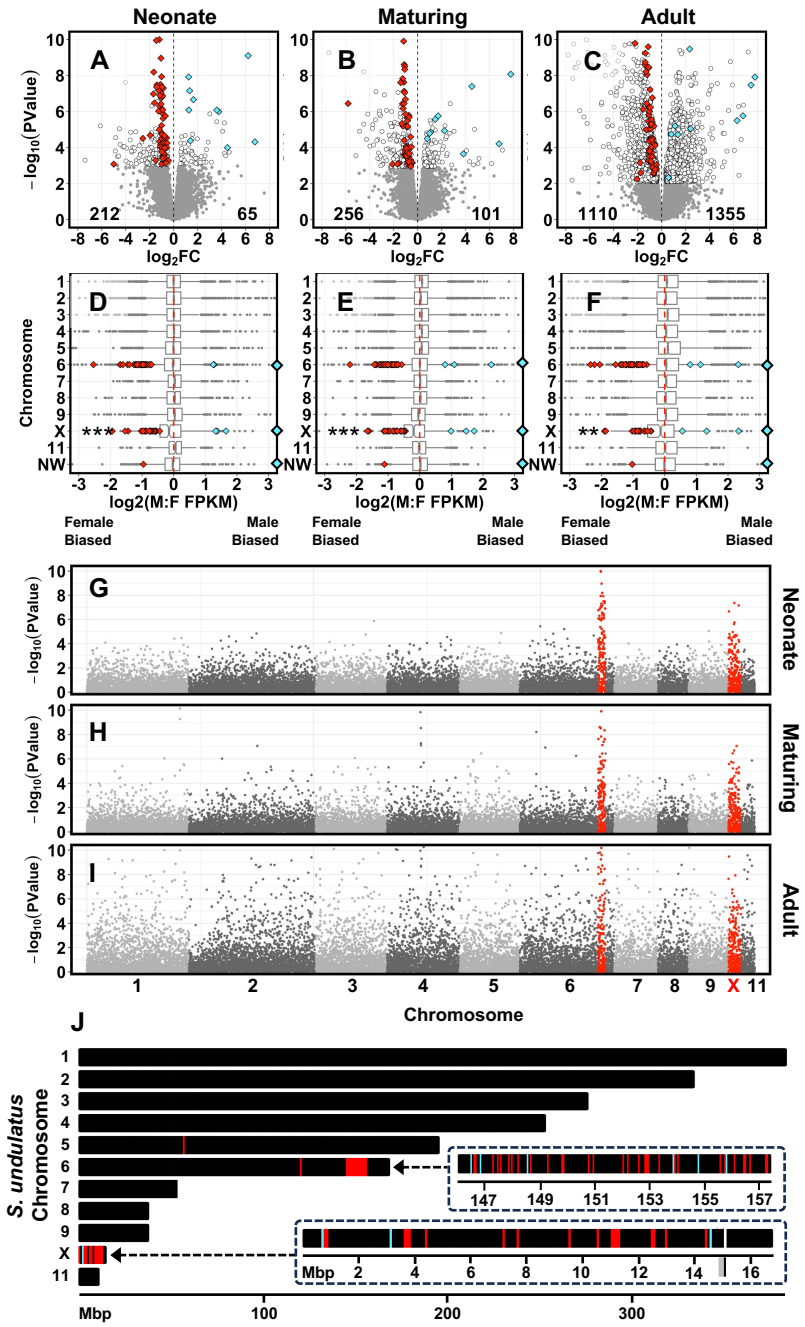

1089

1090 **Figure 4. (A-C)** Volcano plots depicting the magnitude ($\log_2$ fold change) and significance (-

1091 $\log_{10} P$ value) of sex-biased expression across 15,493 genes in liver of *S. jarrovii.* Genes with

1092 significantly (FDR < 0.05) sex-biased expression (DEGs) are indicated in white, with the number

1093 of female-biased and male-biased DEGs indicated in the bottom corners of each panel. DEGs
1094 with consistently sex-biased expression across all ages are shown as red (female-biased) or blue
1095 (male-biased) diamonds. Grey points depict genes that are not significantly sex-biased. (**D-F**)
1096 Boxplots depicting the median (line), interquartile range (box) and the smallest or largest values
1097 within 1.5 x IQR (whiskers) for sex-biased expression ($\log_2$ male:female ratio of fragments per
1098 kilobase per million mapped reads, FPKM) from each of the 11 largest scaffolds and pooled
1099 genes from unplaced scaffolds (NW) in the *S. undulatus* genome. Diamonds indicate consistently
1100 female-biased (red) and male-biased (blue) DEGs, which map predominantly to chromosome 6,
1101 chromosome 10 (X), and unplaced scaffolds (NW). Diamonds on plot borders indicate genes
1102 beyond x-axis limits. Asterisks indicate that median chromosome expression deviates
1103 significantly from balanced male:female expression using Wilcoxon rank sum testing (mu = 0)
1104 with correction for multiple tests (* $P < 0.05$ without correction for multiple tests; ** $P < 0.017$,
1105 the critical alpha after Bonferroni correction; *** $P < 0.001$). (**G-I**) Manhattan plots depicting -
1106 $\log_{10} P$ values for sex-biased expression after ordering genes by *S. undulatus* chromosome and
1107 start position. All genes on X and within an ~11 Mpb distal region of chromosome 6 (DR6) are
1108 shown in red. (**J**) Locations of consistently sex-biased DEGs in *S. jarrovii* when mapped to the *S.*
1109 *undulatus* genome. All consistently sex-biased DEGs map to the ancestral X chromosome (the
1110 region of *S. undulatus* chromosome 10 prior to the large tick at 15.1 Mbp in the lower inset) or
1111 the distal ~11 Mbp region of chromosome 6 (DR6, upper inset), suggesting that this region of *S.*
1112 *undulatus* chromosome 6 is X-linked in *S. jarrovii*.

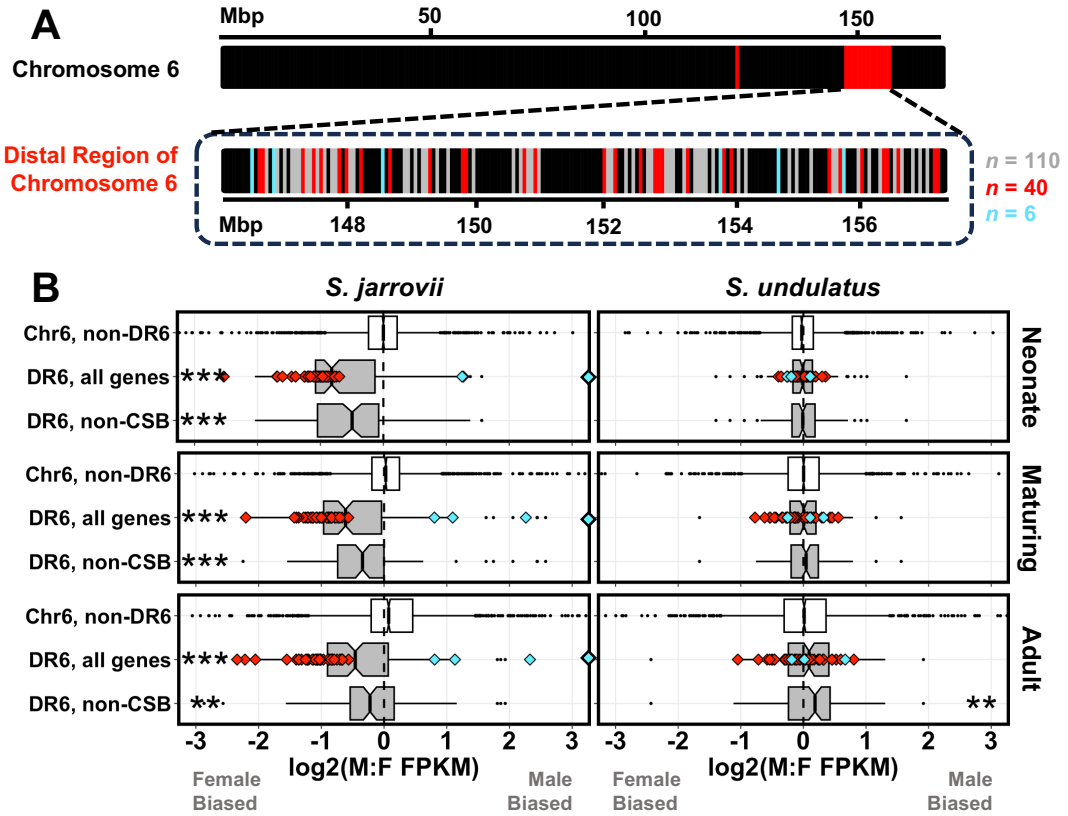

Figure 5. (**A**) Location of consistently female-biased (red), male-biased (blue), and unbiased genes (gray) in *S. jarrovii* that map to the distal region of chromosome 6 (DR6) in *S. undulatus*. Bars are not drawn to scale for gene length. (**B**) Boxplots depicting median (line), interquartile range (box), and 1.5 x IQR (whiskers) for sex-biased expression ($\log_2$ male:female ratio of fragments per kilobase per million mapped reads, FPKM) in liver of *S. jarrovii* and *S. undulatus* at three ages. Boxplots are show for all genes on chromosome 6 except those within DR6 ("Chr 6, non-DR6"), for all genes within DR6 ("DR6, all genes"), and for all genes within DR6 excluding consistently sex-biased DEGs ("DR6, non-CSB"). Diamonds depict consistently sex-biased DEGs with those on plot borders indicating sex bias beyond axis limits. Asterisks indicate when median expression differs from zero using Wilcoxon signed-rank tests with Bonferroni

correction for 2 tests per age (* 0.025 > P > 0.001; ** 0.001 > P > 0.0001; *** P < 0.0001).

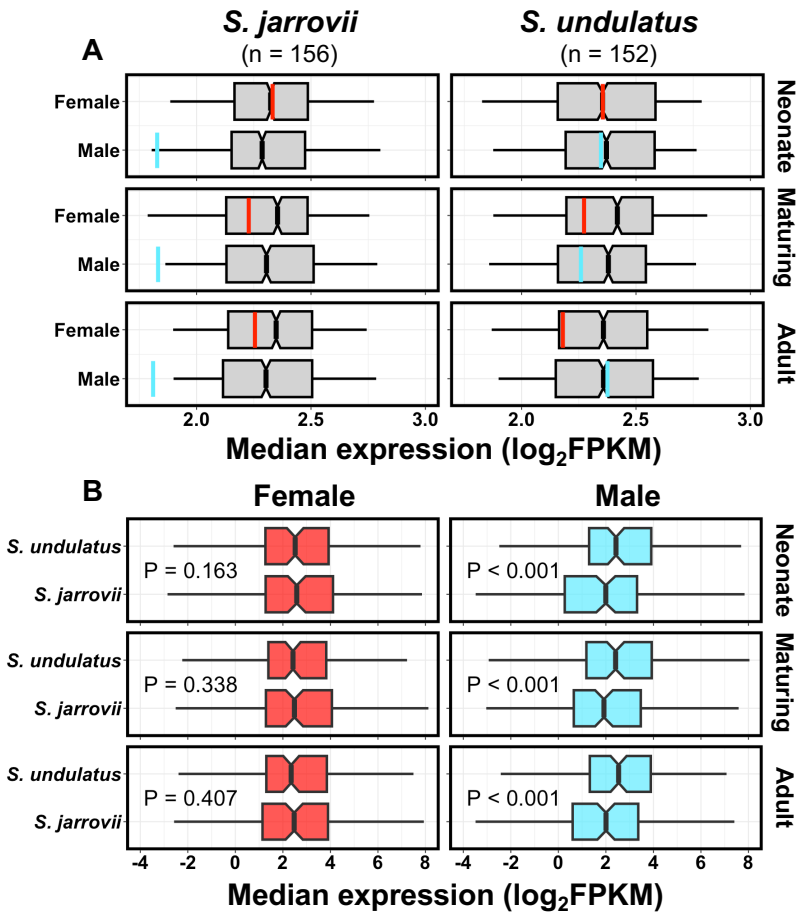

Figure 6. (**A**) Median expression of genes in the distal region of *S. undulatus* chromosome 6 (DR6) versus a sampled distribution of median autosomal expression for each sex across three ages in *S. jarrovii* and *S. undulatus*. Boxplots depict the median (line), intraquartile range (box), and 5th and 95th quantiles for median expression values from 1000 randomly sampled blocks of *n* contiguous autosomal genes (*n* = number of expressed genes within DR6 in each species). Vertical red (female) and blue (male) lines indicate median expression of all genes within DR6. (**B**) Comparisons (paired *t*-test by gene) of expression for all genes on DR6 between *S. jarrovii* and *S. undulatus,* conducted separately by sex. Boxplots depict median (line), intraquartile range (box), and 2.5th and 97.5th quantiles for expression of 152 genes present on DR6 in both species.

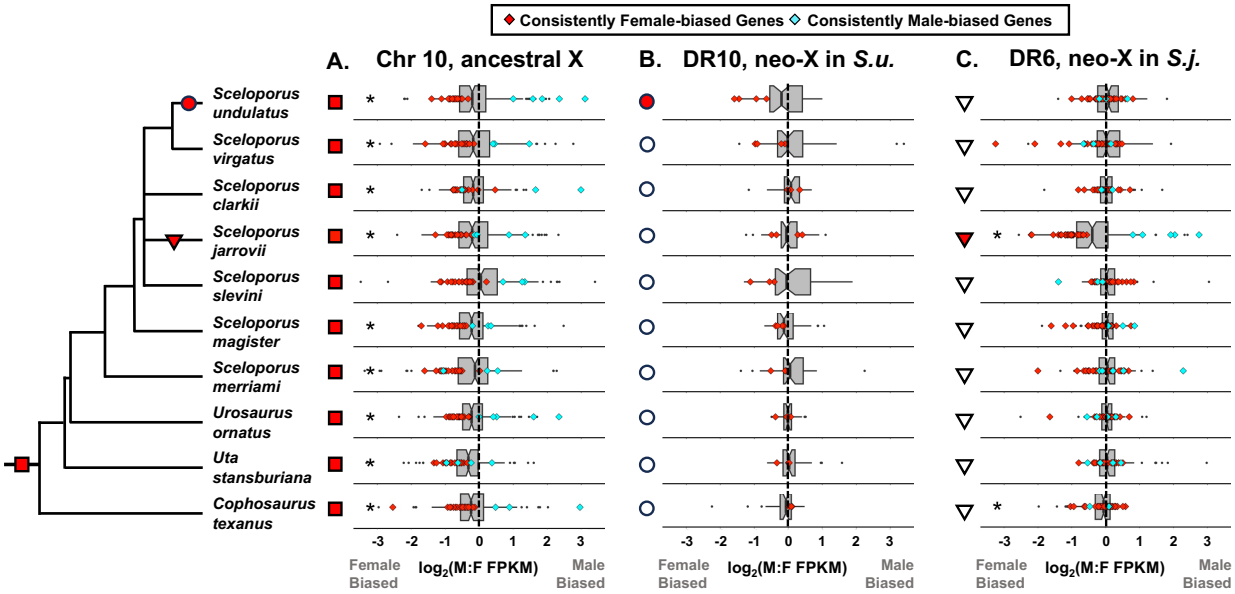

Figure 7. Evolutionary patterns in sex-biased expression of (**A**) the 14.85-Mbp region of *S. undulatus* chromosome 10 that is hemizygous in males (putative ancestral X), (**B**) the distal 1.76-Mbp region of chromosome 10 (DR10, putative neo-X region in *S. undulatus*), and (**C**) the distal 11-Mbp region of chromosome 6 (DR6, putative neo-X region in *S. jarrovii*) based on adult liver transcriptomes from 10 phrynosomatid species mapped to the *S. undulatus* assembly. Boxplots depict the median (line), intraquartile range (box), and 1.5 x IQR (whiskers) of $\log_2$ male:female expression (FPKM) for all expressed genes within each region. Diamonds indicate consistently female-biased (red) and male-biased (blue) genes in transcriptomes from *S. undulatus* (**A-B**) or *S. jarrovii* (**C**). Notches in boxplots indicate 95% confidence intervals of the median. Asterisks denote whether median expression ratios differ significantly from zero (Wilcoxon signed-rank test, Bonferroni-adjusted alpha = 0.005). Red symbols to the left of each boxplot indicate when consistently female-biased DEGs from *S. undulatus* (**A-B**) or *S. jarrovii* (**C**) differ from zero in each species (Wilcoxon signed-rank test, Bonferroni-adjusted alpha = 0.005) and are used to map ancestral (X) and derived (neo-X) male-female expression imbalances onto the phylogeny.